

Granulin loss of function in human mature brain organoids implicates astrocytes in TDP-43 pathology

Martina de Majo,^{1,2,15,*} Mark Koontz,^{1,2,15} Elise Marsan,³ Nir Salinas,¹ Arren Ramsey,³ Yien-Ming Kuo,¹ Kyounghee Seo,¹ Huinan Li,¹ Nina Dräger,⁴ Kun Leng,^{4,5} Santiago L. Gonzales,¹ Michael Kurnellas,⁶ Yuichiro Miyaoka,^{7,8} Joseph R. Klim,^{9,10,11} Martin Kampmann,^{4,12} Michael E. Ward,¹³ Eric J. Huang,^{3,14} and Erik M. Ullian^{1,14,*}

¹Department of Ophthalmology, University of California San Francisco, San Francisco, CA 94143, USA

²Synapticure Inc, Chicago, IL 60612, USA

³Department of Pathology, University of California San Francisco, San Francisco, CA 94143, USA

⁴Institute for Neurodegenerative Diseases, University of California, San Francisco, San Francisco, CA, USA

⁵Medical Scientist Training Program, University of California, San Francisco, San Francisco, CA, USA

⁶Alector, Inc, South San Francisco, CA 94080, USA

⁷Regenerative Medicine Project, Tokyo Metropolitan Institute of Medical Science, 2-1-6 Kamikitazawa, Setagaya, Tokyo 156-8506, Japan

⁸Gladstone Institutes, San Francisco, CA 94158, USA

⁹Department of Stem Cell and Regenerative Biology, Harvard University, Cambridge, MA 02138, USA

¹⁰Stanley Center for Psychiatric Research, Broad Institute of MIT and Harvard, Cambridge, MA 02142, USA

¹¹Harvard Stem Cell Institute, Harvard University, Cambridge, MA 02138, USA

¹²Department of Biochemistry and Biophysics, University of California, San Francisco, San Francisco, CA, USA

¹³National Institute of Neurological Disorders and Stroke, National Institutes of Health, Bethesda, MD, USA

¹⁴Neuroscience Graduate Program, University of California San Francisco, San Francisco, CA 94158, USA

¹⁵These authors contributed equally

*Correspondence: martina@synapticure.com (M.d.M.), erik.ullian@ucsf.edu (E.M.U.)

<https://doi.org/10.1016/j.stemcr.2023.01.012>

SUMMARY

Loss of function (LoF) of TAR-DNA binding protein 43 (TDP-43) and mis-localization, together with TDP-43-positive and hyperphosphorylated inclusions, are found in post-mortem tissue of amyotrophic lateral sclerosis (ALS) and frontotemporal dementia (FTD) patients, including those carrying LoF variants in the progranulin gene (*GRN*). Modeling TDP-43 pathology has been challenging *in vivo* and *in vitro*. We present a three-dimensional induced pluripotent stem cell (iPSC)-derived paradigm—mature brain organoids (mbOrg)—composed of cortical-like-astrocytes (iA) and neurons. When devoid of *GRN*, mbOrgs spontaneously recapitulate TDP-43 mis-localization, hyperphosphorylation, and LoF phenotypes. Mixing and matching genotypes in mbOrgs showed that *GRN*^{-/-} iA are drivers for TDP-43 pathology. Finally, we rescued TDP-43 LoF by adding exogenous progranulin, demonstrating a link between TDP-43 LoF and progranulin expression. In conclusion, we present an iPSC-derived platform that shows striking features of human TDP-43 proteinopathy and provides a tool for the mechanistic modeling of TDP-43 pathology and patient-tailored therapeutic screening for FTD and ALS.

INTRODUCTION

Frontotemporal dementia (FTD) and amyotrophic lateral sclerosis (ALS) are two fatal neurodegenerative diseases. ALS is estimated to affect 2.1 cases per 100,000 people per year (Chiò et al., 2013), while FTD is the second most common cause of dementia for people under 65 years of age (Knopman and Roberts, 2011). ALS and FTD are now thought to be different manifestations of the same disease spectrum, with ALS primarily affecting the motor system and FTD presenting with a variety of symptoms affecting behavioral, executive, language, and motor functions. The two clinical entities can also occur in the same patients, with approximately 10%–15% of ALS patients diagnosed with FTD features (FTD-ALS) and approximately 50% of ALS patients developing some cognitive impairment (Burrell et al., 2016). TAR DNA binding protein (*TARDBP*) gene encodes for the TDP-43 protein, which plays a pivotal

role in these two devastating neurodegenerative disorders. TDP-43 was also recently implicated in limbic-predominant age-related TDP-43 encephalopathy (LATE) (Nelson et al., 2022). Although TDP-43 is an RNA/DNA binding protein that physiologically resides in the nucleus, hyperphosphorylated extranuclear inclusions are found in neuronal cells of approximately 45% of patients with FTD and approximately 97% of patients with ALS (Ling et al., 2013; Neumann et al., 2006). Loss of nuclear TDP-43 results in defective splicing of several transcripts, among which the most thoroughly described is the cryptic splicing of *Stathmin 2* (*STMN2*), a neuron-specific gene important for neuronal survival (Akiyama et al., 2022; Klim et al., 2019; Melamed et al., 2019; Prudencio et al., 2020).

Approximately 5%–10% of all FTD patients harbor mutations in the granulin (*GRN*) gene. (Baker et al., 2006; Cruts et al., 2006; Seelaar et al., 2008). *GRN* transcripts are composed of 13 exons and encode for the progranulin

(PGRN) protein, a highly conserved, approximately 80-kDa protein involved in lysosomal function, neuronal survival, and inflammation (Rhinn et al., 2022). The vast majority of the *GRN* mutations are dominant heterozygous loss-of-function variants that lead to haploinsufficiency with a consequent lower expression of PGRN. These patients have been reported to harbor TDP-43 proteinopathy in their frontal and/or temporal lobes at post-mortem examination (Baker et al., 2006; Mackenzie, 2007). The *GRN* gene has been further linked to Alzheimer's disease and LATE, suggesting that this gene plays roles in multiple neurodegenerative diseases (Bellenguez et al., 2020; Nelson et al., 2019; Viswanathan et al., 2009)

To date, modeling TDP-43 proteinopathy *in vitro* or *in vivo* has been a challenge, with most *in vitro* models applying exogenous stress to replicate pathology akin to what is observed in post-mortem ALS/FTD central nervous system (CNS) tissue. Within these paradigms, induced pluripotent stem cells (iPSCs) hold great promise; they allow for patient- and tissue-specific human-derived *in vitro* models, which can be used for therapeutic screening and phenotype testing (Palomo et al., 2019). As an example, recent work has established the usefulness of iPSC models for the study of *GRN* loss of function (LoF) (Lee and Huang, 2017; Rosen et al., 2011). *GRN* depletion in human iPSC-derived neurons causes cell autonomous changes in signaling (Almeida et al., 2012) and cellular stress (Rosen et al., 2011). Interestingly, these *in vitro* studies did not replicate the characteristic TDP-43 pathology observed in patients (Ahmed et al., 2010; Ward et al., 2014). One possible explanation for this is the fact that *GRN* is also expressed in glia, such as microglia and astrocytes, raising the likelihood that *GRN* LoF causes pathology in a non-cell autonomous manner (Kelley et al., 2018; Zhang et al., 2014; 2016). Recent studies have further implicated glial cells, including astrocytes and microglia, in neurodegenerative disease progression (Desai et al., 2010; Hansen et al., 2018; Verkhratsky et al., 2010). Indeed, several lines of evidence from *GRN* knockout mouse models indicate PGRN deficiency induces glial complement activation and non-autonomous microglia-mediated synaptic pruning that subsequently leads to neurodegeneration (Lui et al., 2016). The role of astrocytes, however, has been less thoroughly characterized and important questions remain, such as whether disease-associated astrocytes are capable of inducing TDP-43 pathology and whether human models of FTD can show pathology similar to that found in post-mortem human brain.

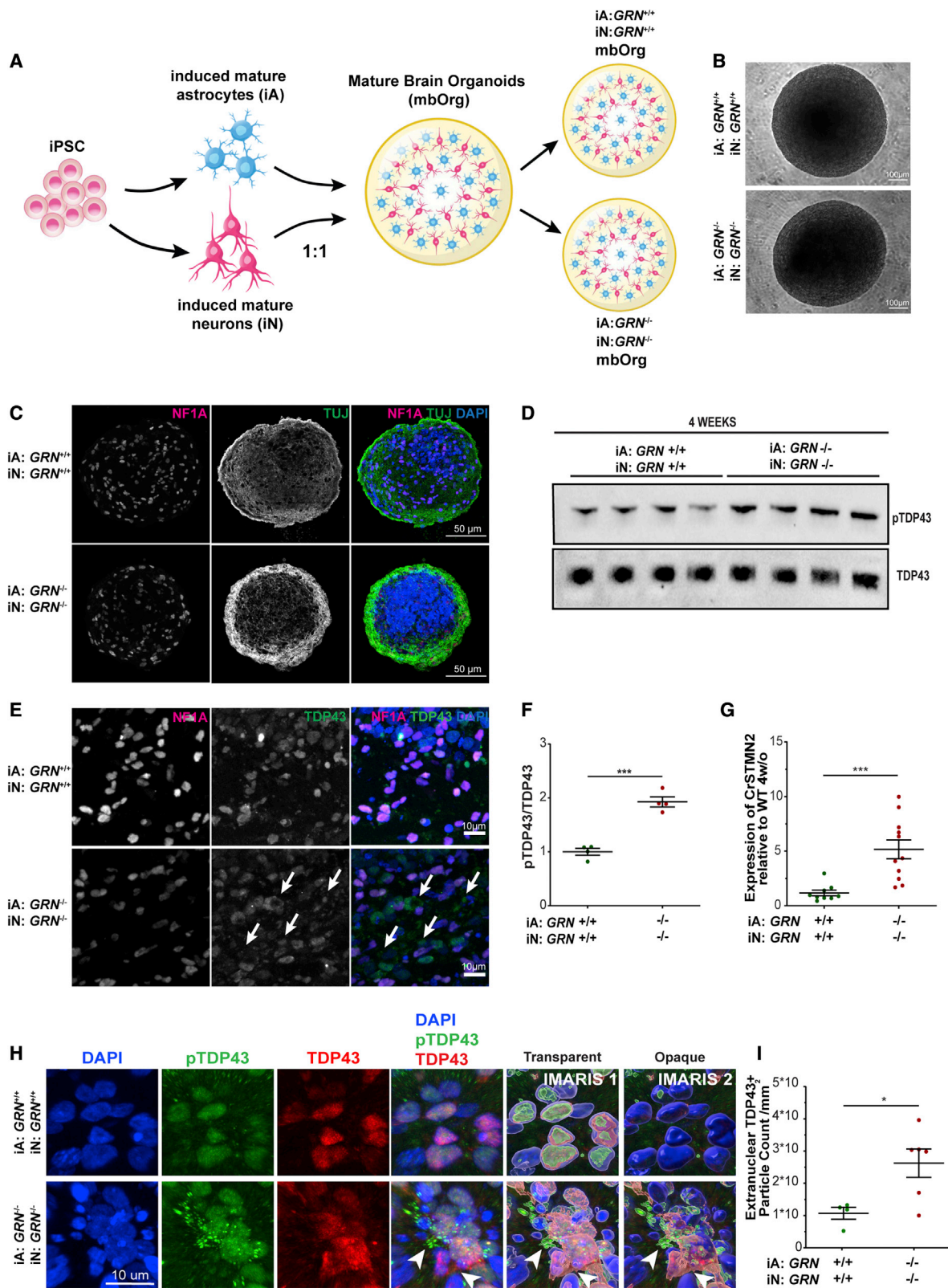
To address this challenge, we applied our previously developed iPSC-derived 3D co-culture model (Krencik et al., 2017; Liu et al., 2020) composed of mature cortical-like neurons and astrocytes, assembled in precise ratios and numbers, to study *GRN* LoF in FTD. When devoid of granulin expression (*GRN*^{-/-}), our model develops features of TDP-43 pathology,

including cryptic *STMN2* (CrSTMN2) splicing, and extranuclear and hyperphosphorylated TDP-43 inclusions. This study presents the first *in vitro* model showing robust evidence of numerous FTD/ALS pathology markers spontaneously developing, overcoming the need of exogenous chemical-induced stress or overexpression. Furthermore, we obtained partial phenotype rescue when *GRN*^{-/-} cells were treated with exogenous full-length PGRN, demonstrating that the development of TDP-43 pathology depends on PGRN expression. We believe this model could provide insight into cell biological mechanisms, leading to TDP-43 pathology and offer a platform for patient-tailored phenotype and therapeutic screening for FTD and ALS patients with suspected or confirmed TDP-43 proteinopathy.

RESULTS

To investigate the role of astrocytes in *GRN* LoF, we modified a previously described protocol to study glial-neuronal interactions (Krencik et al., 2017) (Figure 1A). This approach entails generating neurogenin 2 (NGN2)-inducible cortical-like neurons (iNeurons [iN]), which readily form synapses (Fernandopulle et al., 2018), and mature cortical-like astrocytes (iAstrocytes [iA]) (Krencik et al., 2015; Krencik and Zhang, 2011), and assembling them into three-dimensional (3D) organoid-like structures at defined numbers and ratios of neurons and astrocytes (termed mature brain organoids [mbOrgs]) (Figure 1B). This approach allows us to better model the ratio of astrocytes to neurons thought to comprise the human cortex, as well as mix and match neurons and astrocytes derived from either isogenic wild-type (*GRN*^{+/+}) iPSCs or isogenic *GRN* knockout (*GRN*^{-/-}) iPSCs (Figure S2G). Importantly, *GRN*^{-/-} mbOrgs show a complete loss of PGRN (Figures S1B and S1E). Using this approach, we interrogated the pathological phenotypes of *GRN*^{+/+} and *GRN*^{-/-} mbOrgs. Using transmission light microscopy and confocal imaging, we showed that mbOrgs formed from *GRN*^{+/+} or *GRN*^{-/-} iPSCs both developed into uniform spheres containing a readily detectible array of astrocytes and neurons (Figures 1B and 1C). We first looked at standard markers characteristic of iPSC-derived neurons and astrocytes, by immunostaining. Aquaporin 4 (*AQP4*), an astrocyte specific gene well expressed by astrocytes (Krencik et al., 2015), was strongly and uniformly expressed in both *GRN*^{+/+} and *GRN*^{-/-} mbOrgs (Figure 3A). Similarly, we found a strong and widespread expression of neuronal microtubule-associated protein 2 (*MAP2*) expression in both mbOrgs (Figure 3B). Both results indicate overall stable expression of these astrocyte and neuronal markers in *GRN*^{+/+}, as well as *GRN*^{-/-} mbOrgs.

GRN-associated FTD TDP-43 proteinopathy is characterized by increased levels of phospho-TDP-43 (pTDP-43)



(legend on next page)



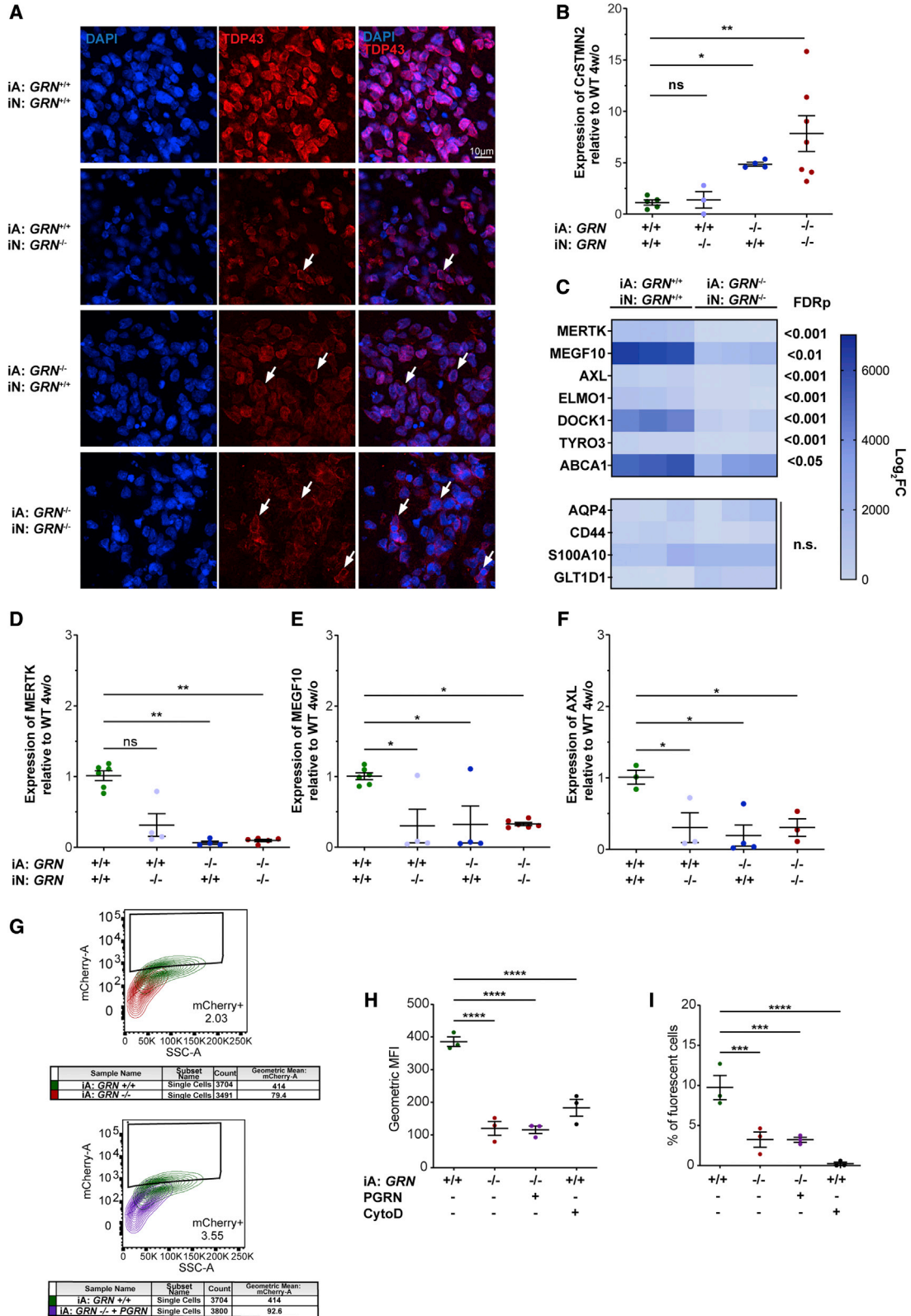
and abnormal TDP-43 cytoplasmic accumulation, seen in postmortem CNS tissue (Baker et al., 2006; Mackenzie, 2007). To assess the TDP-43 pathology in our model, we measured the levels of both pTDP-43, using a ser409/410-specific pTDP-43 antibody, and total TDP-43 by performing western blotting in $GRN^{+/+}$ and $GRN^{-/-}$ mbOrgs lysates after 4 weeks of culture (Figure 1D). Quantification of the pTDP-43 to TDP-43 ratio revealed a clear increase in the phosphorylated form of TDP-43 in $GRN^{-/-}$ mbOrgs (Figure 1F), similar to what has been described in post-mortem tissue (Baker et al., 2006; Mackenzie, 2007). We next performed immunostaining for TDP-43 in sections of 4-week-old mbOrgs and found clear evidence of extranuclear localization of TDP-43 in $GRN^{-/-}$ mbOrgs, but not in $GRN^{+/+}$ mbOrgs, where TDP-43 was mostly co-localized with nuclei (Figure 1E). IMARIS reconstruction and quantification of confocal images from TDP-43 staining demonstrated an increase in extranuclear TDP-43 particle count in $GRN^{-/-}$ mbOrgs (Figures 1H and 1I). Recent work has shown that a key function of TDP-43 in healthy cells is mRNA splicing repression in the nucleus, whereas in disease TDP-43 nuclear depletion results in a number of mis-spliced transcripts (Brown et al., 2022). Among these, *STMN2* is the most thoroughly studied; mis-splicing of *STMN2* transcripts (CrSTMN2) has been considered a robust indicator of TDP-43 pathology and correlates with the level of pTDP-43 (Klim et al., 2019; Melamed et al., 2019; Prudencio et al., 2020). Thus, to determine if CrSTMN2 transcripts can be detected in our model system showing TDP-43 mis-localization, we adapted a method (Klim et al., 2019) to develop a sensitive quantitative PCR

(qPCR)-based assay and found a highly significant, approximately 4-fold increase in CrSTMN2 in the $GRN^{-/-}$ versus $GRN^{+/+}$ mbOrgs (Figure 1G). We next asked if these unique features of human neurodegenerative disease progress over time in $GRN^{-/-}$ mbOrgs, as would be expected if these features represent cellular mechanisms that could be relevant to human disease progression. To test this, we looked at an earlier 2-week time point and assessed the presence of these same features that are robustly present at four weeks. We found that, while there was a trend, variable results caused these features to have not yet reached statistical significance at the earlier time point, consistent with a progression of relevant cellular signaling driving these features (Figures S1A, S1C, and S1D). Taken together, these data demonstrate a remarkable degree of human-specific FTD pathological phenotypes recapitulated in the iPSC-derived mbOrg model and are, to the best of our knowledge, the first demonstration of multiple TDP-43-associated pathological phenotypes shown in an unperturbed *in vitro* model system.

These results show that *GRN* LoF in both iPSC-derived neurons and astrocytes in our 3D platform display a remarkable array of phenotypes relevant to FTD-TDP. We next wanted to investigate if *GRN* LoF is required in both cell types or if we can detect evidence of pathology when either neurons or astrocytes are $GRN^{-/-}$. To investigate this, we took advantage of the assembled nature of the mbOrgs and made heterotypic cultures containing all possible combinations of $GRN^{-/-}$ or $GRN^{+/+}$ neurons + $GRN^{-/-}$ or $GRN^{+/+}$ astrocytes (either $GRN^{-/-}$ neurons + $GRN^{+/+}$ astrocytes or $GRN^{+/+}$ neurons + $GRN^{-/-}$ astrocytes, along with the control

Figure 1. $GRN^{-/-}$ mbOrgs show features of human TDP-43 proteinopathy after 4 weeks in culture

- (A) Diagram showing the process by which mbOrgs are differentiated and assembled. Briefly, iPSCs are differentiated into mature cortical-like astrocytes and neurons and assembled in a 1:1 ratio in 3D co-cultures called mbOrg. The mbOrg are grown for four weeks and then analyzed.
- (B) Brightfield image of two mbOrgs ($GRN^{+/+}$, $GRN^{-/-}$) kept in culture for 4 weeks (scale bar, 100 μ m).
- (C) Confocal images of mbOrg slices ($GRN^{+/+}$ or $GRN^{-/-}$) showing expression of NF1A, TUJ, and DAPI after 4 weeks in culture (scale bar, 50 μ m).
- (D) Western blot of mbOrgs whole lysate showing higher expression of pTDP-43 in $GRN^{-/-}$ compared with $GRN^{+/+}$ mbOrgs when normalized to total TDP-43.
- (E) Western blot quantification showing significantly higher expression of pTDP-43 in $GRN^{-/-}$ compared with $GRN^{+/+}$ mbOrgs when normalized to total TDP-43 ($n = 4$, unpaired t test, two tailed, $p < 0.001$, each n represents approximately 50 mbOrgs and was repeated independently four times).
- (F) Confocal images of mbOrg slices ($GRN^{+/+}$ or $GRN^{-/-}$) showing expression of NFIA, TDP-43 and DAPI after 4 weeks in culture (scale bar, 10 μ m).
- (G) Quantification of CrSTMN2 expression using qPCR showing significantly higher expression in $GRN^{-/-}$ compared to $GRN^{+/+}$ mbOrgs ($n = 11 \pm$, unpaired t test, two tailed, $p \leq 0.001$, each n represents approximately 50 mbOrgs and the experiment was repeated independently four times).
- (H) IMARIS 3D reconstruction of TDP-43 and pTDP-43 staining in 4-week-old mbOrgs (scale bar, 10 μ m).
- (I) quantification of extranuclear TDP-43 particle count per square millimeter, showing significantly higher count in $GRN^{-/-}$ compared with $GRN^{+/+}$ mbOrgs. Each dot represents one independent mbOrg ($GRN^{+/+}$ $n = 4$, $GRN^{-/-}$ $n = 6$, unpaired t test, two tailed, $p < 0.05$, each n is one mbOrg and the experiment was repeated independently three times). For all graphs, data are presented as mean \pm standard error of the mean.



(legend on next page)



both-cell-type $GRN^{+/+}$ and both-cell-type $GRN^{-/-}$ mbOrgs). Immunostaining for TDP-43 showed expected pathology in the both-cell-type $GRN^{-/-}$ mbOrgs. We also found TDP-43 pathology in the $GRN^{+/+}$ neurons + $GRN^{-/-}$ astrocytes mbOrgs (Figure 2A). To further quantitatively examine the heterotypic cultures, we assessed CrSTMN2. As expected, quantification of CrSTMN2 showed the most severe phenotype in both-cell-type $GRN^{-/-}$ mbOrgs. Surprisingly, we found a robust CrSTMN2 increase in $GRN^{+/+}$ neurons + $GRN^{-/-}$ astrocytes mbOrgs (Figure 2B), but not in $GRN^{-/-}$ neurons + $GRN^{+/+}$ astrocytes mbOrgs, confirming what was observed by immunocytochemistry. These results demonstrate that $GRN^{-/-}$ astrocytes are sufficient to induce robust TDP-43 and CrSTMN2 phenotypes in mbOrgs, even in the presence of $GRN^{+/+}$ neurons, and indicate that the diseased human astrocytes can drive neurodegenerative phenotypes in healthy human neurons.

To further characterize the effect of GRN LoF on iA, we performed bulk RNA sequencing (Figures 2D and 2E) to examine gene expression in $GRN^{+/+}$ and $GRN^{-/-}$ mbOrgs after 4 weeks in culture. Interestingly, we found that a set of astrocyte genes known to be involved in phagocytosis (Figure 2C upper panel), but not other astrocyte specific marker genes, were down-regulated in the $GRN^{-/-}$ mbOrgs at 4 weeks when compared with $GRN^{+/+}$ mbOrgs (Figure 2C lower panel). Confirmation with qPCR shows MER proto-oncogene, tyrosine kinase (MERTK), multiple EGF-like domains 10 (MEGF10), and AXL receptor tyrosine kinase (AXL) down-regulation in $GRN^{-/-}$ mbOrgs. Interestingly,

all three phagocytosis-related genes were also significantly down-regulated in mbOrgs composed of $GRN^{+/+}$ neurons + $GRN^{-/-}$ astrocytes. For the $GRN^{-/-}$ neurons + $GRN^{+/+}$ astrocytes mbOrgs, both MEGF10 and AXL were significantly down-regulated and there was a non-significant trend for down-regulation for MERTK (Figures 2D–2F). These results suggest that GRN LoF in astrocytes and/or neurons can lead to a down-regulation of phagocytosis-related astrocyte genes. To directly assess the functional consequences of GRN loss in astrocytes, we performed a synaptosome phagocytosis assay in $GRN^{+/+}$ or $GRN^{-/-}$ astrocytes two-dimensional (2D) cultures. The results point to a profound deficit in synaptosome phagocytosis in the $GRN^{-/-}$ astrocytes (Figures 2G–2I). We attempted to rescue this deficit with the addition of recombinant PGRN; however, the tested conditions were not sufficient to revert the phagocytosis deficit (Figures 2G–2I). A similar treatment with PGRN in 2D astro-neuronal cultures for up to 4 weeks failed to rescue the phagocytosis-related down-regulated genes MERTK and MEGF10 (Figures 1H and 1K). Overall, these data show that GRN LoF leads to changes in astrocyte phagocytosis and that the genes associated with astrocyte phagocytosis are regulated both cell autonomously and non-cell autonomously.

Previous work has uncovered a critical role for astrocyte phagocytosis in regulating synapses in various regions of the mouse CNS with specific involvement of MERTK and MEGF10 (Chung et al., 2013). We wondered whether the deficits we observed in $GRN^{-/-}$ astrocyte

Figure 2. $GRN^{-/-}$ mature astrocytes drive *STMN2* mis-splicing in mbOrgs and show evidence of defective phagocytosis

(A) Qualitative immunohistochemistry of mbOrg slices (GRN iA: +/+ iN: +/+, GRN iA: +/+ iN: -/-, GRN iA: -/- iN: +/+, GRN iA: -/- iN: -/-) showing expression of TDP-43 and DAPI after four weeks in culture (scale bar, 10 μ m).

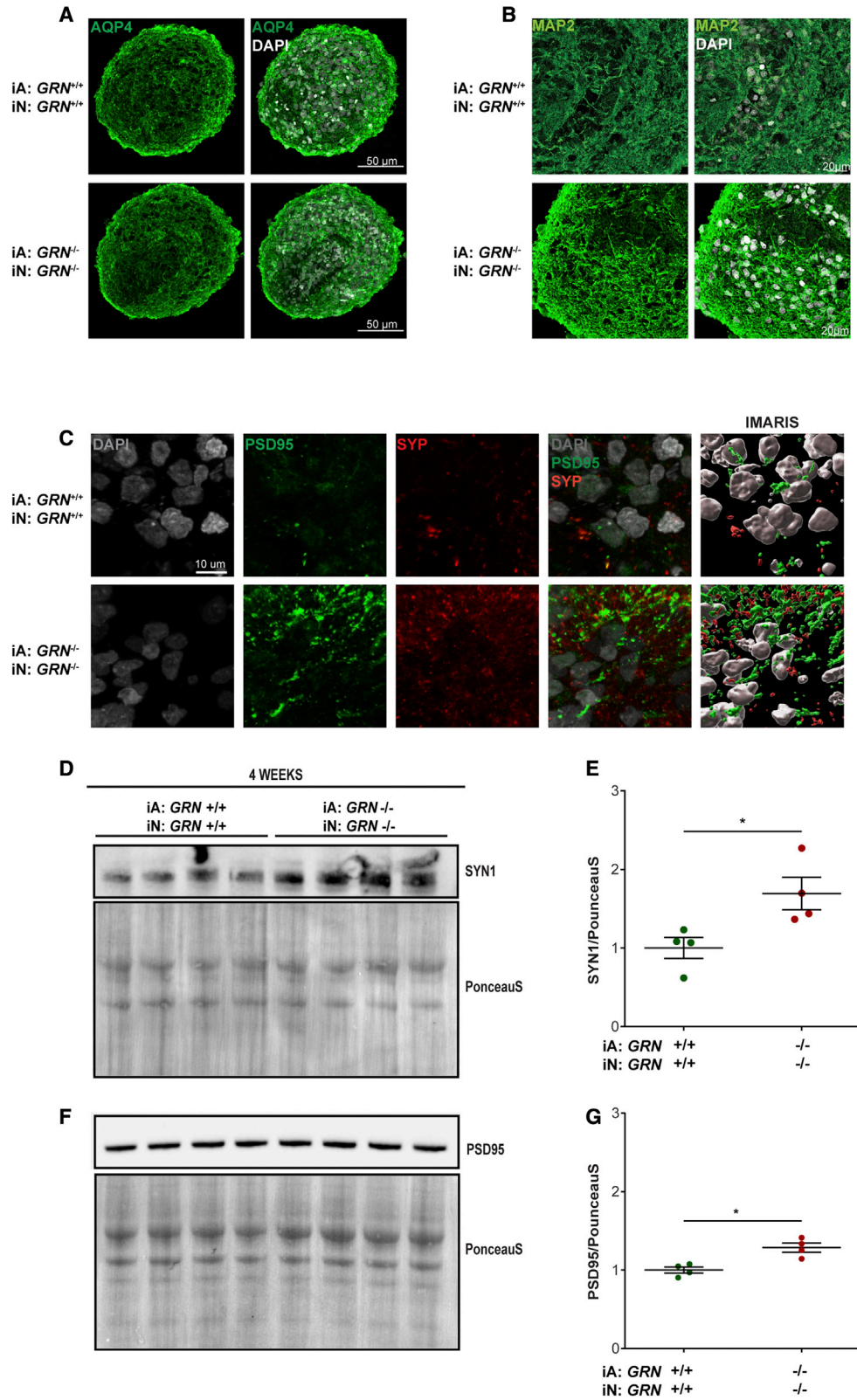
(B) Quantification of CrSTMN2 expression using qPCR showing increasingly significant CrSTMN2 expression in GRN iA: -/- iN: +/+ and GRN iA: -/- iN: -/- compared with GRN iA: +/+ iN: +/+ and GRN iA: +/+ iN: -/- mbOrgs (n = 4, one-way ANOVA followed by multiple comparison, *p < 0.05 **p < 0.005, each n represents approximately 50 mbOrgs and the experiment was repeated independently three times).

(C) At the top, expression heatmap showing bulk RNA sequencing values of seven genes linked to phagocytosis in 4-week-old mbOrgs. All the genes listed here are differentially expressed in the $GRN^{+/+}$ samples versus $GRN^{-/-}$ samples. Specifically, all the genes listed here are less expressed in the 4-week-old $GRN^{-/-}$ compared with the $GRN^{+/+}$ mbOrgs (false discovery rate [FDR] < 0.05, n = 3). At the bottom expression heatmap of astrocyte markers that are not differentially expressed in the 4-week-old $GRN^{-/-}$ compared with the $GRN^{+/+}$ mbOrgs. Fold change (FC).

(D–F) qPCR analysis of three (MERTK, MEGF10, and AXL) of the seven phagocytosis markers analyzed with RNA sequencing in all four conditions: GRN iA: +/+ iN: +/+, GRN iA: +/+ iN: -/-, GRN iA: -/- iN: +/+, GRN iA: -/- iN: -/- (n = 4, one-way ANOVA followed by multiple comparison, *p < 0.05 **p < 0.005 each n represents approximately 50 mbOrgs and the experiment was repeated independently three times).

(G) Graphic representation of the clustering analysis depicting the changes of phagocytic activity in the different conditions (iA $GRN^{+/+}$ in green, iA $GRN^{-/-}$ in red and iA $GRN^{-/-}$ + PGRN in purple). Cells were treated with mCherry labeled rat synaptosome and analyzed at the cytofluorimeter as described in Dräger et al., 2022.

(H, I) Quantification of FACS analysis showing geometric mean fluorescence intensity (MFI) and percentage of fluorescent cells phagocytosed by the mature astrocytes. iA $GRN^{-/-}$ and iA $GRN^{-/-}$ + PGRN phagocyte significantly lower amount of mCherry-labeled synaptosome according to both parameters compared to iA $GRN^{+/+}$ (n = 3, one-way ANOVA followed by multiple comparison, ***p < 0.0005 ****p < 0.00005 each n represents approximately 250,000 cells and the experiment was repeated independently three times). Negative control showed in black (iA $GRN^{+/+}$ treated with cytoD). For all graphs, data are presented as mean \pm standard error of the mean.



(legend on next page)



phagocytosis may be associated with corresponding increases in synapses in our model. Therefore, we looked for any synaptic phenotypes associated with loss of phagocytosis in the mbOrgs. First, we immunostained mbOrgs for the presynaptic marker synaptophysin (SYP) and post-synaptic marker post-synaptic density protein 95 (PSD-95). Confocal microscopy analysis and IMARIS 3D reconstruction showed that in comparison with 4-week-old $GRN^{+/+}$ mbOrgs, $GRN^{-/-}$ mbOrgs contain more SYP and PSD-95 puncta (Figure 3C). We next wanted to quantitatively assess the expression levels of synaptic markers and performed western blotting for both pre- and post-synaptic markers synapsin and PSD-95, respectively. The results revealed an increase in both pre- and post-synaptic protein in the $GRN^{-/-}$ mbOrgs (Figures 3D and 3E). Thus, GRN loss is associated with effects on synapses consistent with previous studies (Petoukhov et al., 2013; Tapia et al., 2011; Uesaka et al., 2018; L. Wang et al., 2022).

Overall, these findings indicate that $GRN^{-/-}$ astrocytes are likely sufficient to induce TDP-43 pathology, as well as a significant increase in CrSTMN2 in neurons in the 3D mbOrgs. We then decided to investigate whether the same two findings are present in a 2D culture system. We performed the co-culture experiments as illustrated in Figure 4A. Both $GRN^{+/+}$ and $GRN^{-/-}$ co-cultures of astrocytes and neurons look uniformly healthy at 4 weeks (28 DIV) (Figure 4B). When immunostained for MAP2, both cultures showed robust and extensive dendritic arbors (Figure 4B). As previously reported, staining for TDP-43 and pTDP-43 failed to show an overt pathological TDP-43 associated signal. Furthermore, western blot analyses for the ratio of pTDP-43 to total TDP-43 showed no significant increase at 4 weeks in $GRN^{-/-}$ 2D co-cultures. We then assessed the expression of CrSTMN2 in the 2D co-cultures. We found a significant increase in the expression of CrSTMN2 at 4 weeks in 2D co-cultures of $GRN^{-/-}$ astrocytes with $GRN^{-/-}$ neurons (Figure 4G). This result led us to investigate whether this more subtle TDP-43-associated phenotype might be reversible. Although phenotypes are not as severe in the 2D co-culture, they are amenable to exogenous compound rescue experiments. As proof of

principle, we tried rescuing the CrSTMN2 phenotype by treating the cells with recombinant PGRN. We first determined what, if any, concentration of PGRN shows clear cellular uptake. We determined by immunostaining that 1 $\mu\text{g}/\text{mL}$ recombinant PGRN fed every 3 days for 28 days leads to a robust rescue of PGRN deficiency in $GRN^{-/-}$ neuronal and $GRN^{-/-}$ astrocytes cell bodies (Figure 4F). We next examined CrSTMN2 in PGRN-treated cells versus control and found a consistent and significant rescue of CrSTMN2 in 2D co-cultures of $GRN^{-/-}$ astrocytes and $GRN^{-/-}$ neurons (Figure 4G). These are, to our knowledge, the first data demonstrating a rescue of GRN LoF CrSTMN2 expression increases.

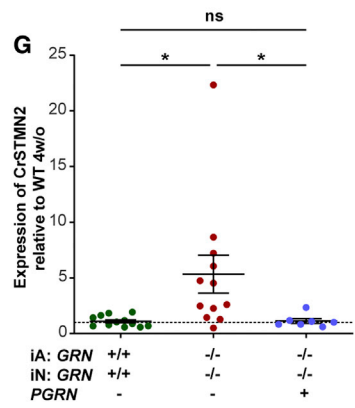
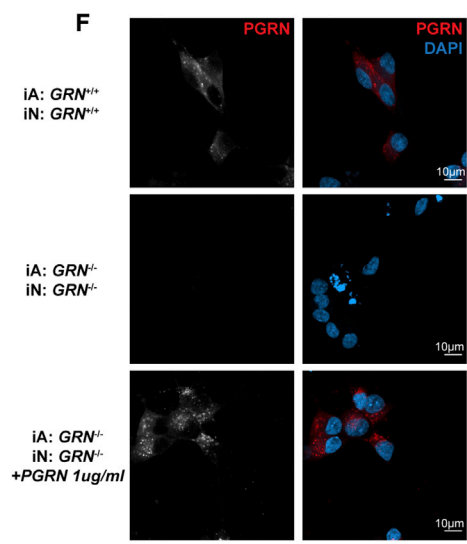
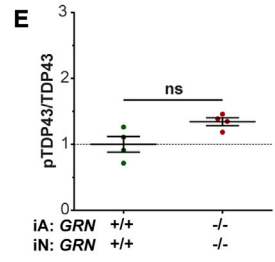
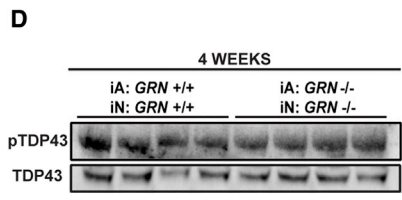
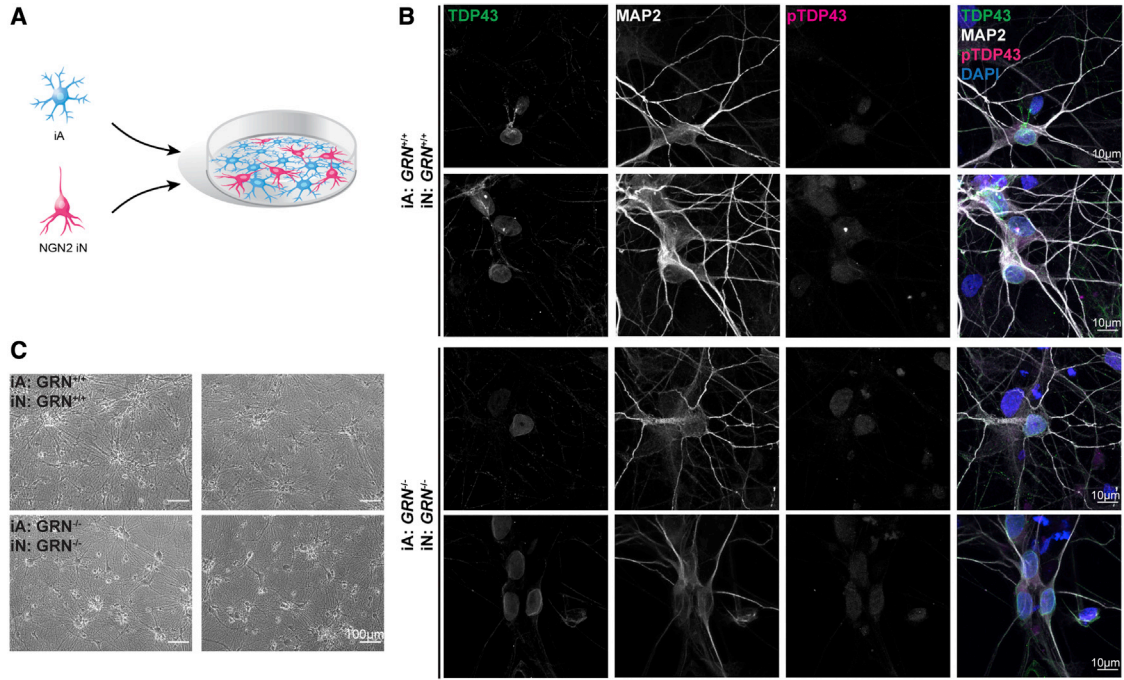
DISCUSSION

Here, we characterize an *in vitro* human iPSC-derived neuro-glia 3D model of TDP-43 proteinopathy in a context of PGRN deficiency. While iPSC-induced neurons have provided numerous cell-autonomous biological insights into neurodegeneration, most models do not recapitulate multiple aspects of TDP-43-associated pathology. These phenotypic challenges have made therapeutic discovery difficult for TDP-43 proteinopathies (Buratti, 2020). Our focus on iPSC neuron-glia interactions have yielded a 3D paradigm spontaneously reproducing overt pathological features of TDP-43 proteinopathy. Interestingly, while TDP-43 proteinopathy was not noticeable in 2D co-culture, TDP-43 LoF characterized by *STMN2* mis-splicing was recapitulated in both 2D and 3D co-culture models.

Our approach is distinct in that we use a simple, reproducible, and straightforward engineered system to model spontaneous TDP-43 pathology. Indeed, our 3D iPSC-induced cortical-like neuron and astrocyte co-culture with GRN loss strikingly and consistently recapitulated human specific TDP-43 cell pathology reported in human FTD patient brain. Importantly, these phenotypes are not seen in the same individually cultured iPSC-induced neurons or astrocytes and are much milder in our 2D co-culture paradigm. Similarly, two recent studies highlighted

Figure 3. $GRN^{-/-}$ mbOrgs show higher synaptic density when compared with $GRN^{+/+}$ mbOrg

- (A) Confocal images of mbOrg slices ($GRN^{+/+}$ or $GRN^{-/-}$) showing evenly distributed expression of AQP4 and DAPI (scale bar, 50 μm).
(B) Confocal images of mbOrg slices ($GRN^{+/+}$ or $GRN^{-/-}$) showing evenly distributed expression of MAP2 and DAPI (scale bar, 20 μm).
(C) IMARIS 3D reconstruction of PSD95 and synaptophysin (SYP) staining in 4-week-old mbOrg (scale bar, 10 μm) showing higher synaptic density in $GRN^{-/-}$ compared with $GRN^{+/+}$ mbOrg.
(D, E) Western blot of mbOrg whole lysate showing higher expression on Synapsin1 (SYN1) in $GRN^{-/-}$ compared with $GRN^{+/+}$ mbOrgs when normalized to PonceauS staining and its quantification (E) ($n = 4$, unpaired t test, two tailed, $p < 0.05$, each n represents approximately 50 mbOrgs and was repeated independently four times).
(F, G) Western blot of mbOrgs whole lysate showing higher expression on PSD95 in $GRN^{-/-}$ compared with $GRN^{+/+}$ mbOrgs when normalized to PonceauS staining and its quantification (G) ($n = 4$, unpaired t test, two tailed, $p < 0.05$, each n represents approximately 50 mbOrgs and was repeated independently four times). For all graphs data are presented as mean \pm standard error of the mean.



(legend on next page)



evidence of mild TDP-43 pathology in 2D ALS-iPSC-derived neuron and 100-day-old *GRN* knockout neuronal cultures when compared with healthy controls, with the ALS study showing evidence of *STMN2* mis-splicing (Bosso-lasco et al., 2022; Coyne et al., 2021). The reason for difference in phenotype severity between 2D and 3D co-cultures is not entirely clear, but we have previously found that astrocytes in 3D culture are significantly more complex and resemble the highly complex morphology of human astrocytes *in vivo* (Krencik et al., 2017). Furthermore, these previously published results suggest that control iPSC-derived human astrocytes in 3D are not highly reactive by 4 weeks *in vitro* (Krencik et al., 2015), potentially providing a healthy baseline with which to compare disease-causing mutations.

The data presented here provide strong evidence that *GRN*^{-/-} astrocytes drive *STMN2* mis-splicing in both *GRN*^{-/-} and *GRN*^{+/+} neurons in mbOrg. Indeed, the 3D mbOrgs are advantageous in allowing easy mixing and matching of cellular genotypes with cells used to assemble the cultures. Thus, our ability to generate mixed *GRN*^{+/+} neurons + *GRN*^{-/-} astrocytes showing nearly as strong crSTMN2 and TDP-43 phenotypes of full *GRN*^{-/-} neuron and astrocyte cultures indicate that *GRN* LoF in human astrocytes can lead to TDP-43 LoF in neurons. This finding is mechanistically important and adds to a growing body of literature suggesting that disease-associated astrocytes and more generally glia can drive cell death and neuronal dysfunction (Huang et al., 2022; Leng et al., 2022; Liddel et al., 2017; Taha et al., 2022; Zhang et al., 2020).

Our investigation of phagocytic activity assays in *GRN*^{-/-} iA demonstrated significant deficit when compared with *GRN*^{+/+} iA. Phagocytic changes have been reported in *GRN*^{-/-} microglia (Guan et al., 2020; Lui et al., 2016) and in microglia differentiated from ALS peripheral blood mononuclear cells (PBMCs) when compared with control PBMC-derived microglia (Quek et al., 2022). It has also been shown that diseased-induced astrocytes lose the ability to engulf

synapses and show decreased expression of phagocytosis receptor *MEGF10* and *MERTK* (Liddel et al., 2017). We show that *GRN*^{-/-} iA when cultured in 3D mbOrgs for 4 weeks also display differential expression of phagocytosis markers when compared with *GRN*^{+/+} iA. A significantly lower expression of *MERTK*, *MEGF10*, and *AXL* was confirmed by qPCR in *GRN*^{-/-} iA in both 3D and 2D co-cultures and was not rescued by PGRN treatment. *MEGF10* and *MERTK* have been specifically implicated in synaptic pruning and maturation in both in the developing and adult brain (Chung et al., 2013; Lee and Chung, 2019); their down-regulation could explain the significantly higher expression of pre- and post-synaptic markers observed in our 3D *GRN*^{-/-} mbOrgs when compared with *GRN*^{+/+}. Overall, this model recapitulates key disease astrocyte-like features observed in neurodegenerative disorders; it is, therefore, not surprising that *GRN*^{-/-} iA are able to drive the disease phenotype in mbOrgs even when co-cultured with healthy neurons.

As noted, our use of the mbOrgs revealed a compelling set of FTD-related phenotypes associated with TDP-43 LoF. This finding gave us confidence that the significant crSTMN2 increase in the 2D co-cultures of neurons and astrocytes was caused by the lack of expression of *GRN*. Thus, we tested the ability of recombinant PGRN to rescue this deficit in the context of *GRN*^{-/-} neurons and astrocytes. Our results show a striking ability to rescue crSTMN2 increases in the 2D culture, consistent with this observation being a direct result of loss of *GRN* and subsequent loss of PGRN function. It is important to note that, although treatment with PGRN can rescue crSTMN2 in the 2D co-culture, we did not find that treatment with PGRN was sufficient to rescue the observed phagocytosis deficits in the *GRN*^{-/-} iA. This might be because these astrocytes had been matured for 6–9 months before analysis, so the changes associated with loss of *GRN* may not be acutely rescuable. We believe that the multifunctional PGRN protein is likely to affect numerous aspects of cellular function; some acutely and some chronically. Thus, some deficits may be readily

Figure 4. *STMN2* mis-splicing can be rescued in 2D

- (A) Diagram showing the process by which 2D cultures are made. Briefly, iPSCs are differentiated into mature cortical-like astrocytes and neurons and assembled in a 1:1 ratio in 2D co-cultures. The co-cultures are grown for 4 weeks and then analyzed.
- (B) Representative ICC images of 2D cultures stained for TDP-43, pTDP-43, MAP2, and DAPI (scale bar, 10 μ m).
- (C) Brightfield image of 2D cultures (*GRN*^{+/+}, *GRN*^{-/-}) at the 4-week timepoint (scale bar, 100 μ m).
- (D) Western blot of 2D co-cultures whole lysate of pTDP-43 and total TDP-43 in *GRN*^{+/+} and *GRN*^{-/-} 2D co-cultures.
- (E) Western blot quantification showing similar expression on pTDP-43 in *GRN*^{-/-} compared with *GRN*^{+/+} 2D co-cultures when normalized to total TDP-43 (n = 4, unpaired t test, two tailed, p > 0.05, each n represents approximately 1 \times 10⁶ cells and was repeated independently four times).
- (F) Representative ICC images of 2D cultures stained for PGRN and DAPI showing positive staining in both *GRN*^{+/+} and PGRN treated *GRN*^{-/-} but no PGRN staining in *GRN*^{-/-} co-cultures (scale bar, 10 μ m).
- (G) Quantification of CrSTMN2 expression using qPCR showing significantly higher expression in *GRN*^{-/-} compared with *GRN*^{+/+} 2D co-cultures. The difference is rescued when *GRN*^{-/-} are treated with PGRN for 4 weeks (n = 10, one-way ANOVA followed by multiple comparison, *p < 0.05, ns p > 0.05, each n represents approximately 1 \times 10⁶ cells and was repeated independently three times). For all graphs, data are presented as mean \pm standard error of the mean.



rescued by replacing PGRN and some may not. This is consistent with the recent finding that acute treatment with an engineered PGRN protein rescued some phenotypes of *GRN* deficient microglia, but not all phenotypes associated with *GRN* loss (Logan et al., 2021).

Like all model systems, iPSC-derived models have limitations. In particular, they do not fully recapitulate all features of the complex human brain and they currently do not incorporate microglia or vascular networks, although this may be possible in the future (Blanchard et al., 2021; Kumar et al., 2017; Mantle and Lee, 2018). This paradigm (both in 2D and 3D) is, however, amenable to the addition of any further cell types to make it an even more complete modeling tool. Despite these limitations, this approach provides a simple and straightforward method to model neurodegeneration that can be readily incorporated into laboratories and expanded to study basic cellular interactions and mechanisms of disease, revealing cell autonomous and non-autonomous roles for disease genes in astrocytes and neurons.

EXPERIMENTAL PROCEDURES

Resource availability

Corresponding authors

Further resources and reagents inquiries should be directed to and will be fulfilled by the corresponding authors (erik.ullian@ucsf.edu (martina@synapticure.com)

Materials availability

For questions about materials and methods, please contact with the corresponding authors.

Data and code availability

Analyzed RNA-seq data will be made available upon request. The accession number for the fastq files data reported in this paper is <https://www.ncbi.nlm.nih.gov/sra/PRJNA925944>: SRA number PRJNA925944.

Human iPSC stem cell lines

Isogenic human iPSC line WTC11 and *GRN*^{-/-} iPSC line were generated by Dr. Bruce R. Conklin, as previously described (Miyaoaka et al., 2014). *GRN*^{-/-} iPSC and *GRN*^{-/-} NGN2 iPSC were engineered (Figure S2F) and provided by Dr. Michael E. Ward (NIH) as previously described (Wang et al., 2017). iPSCs were cultured and maintained in Essential 8 Medium (Gibco, A1517001) on 6-well cell culture plates (Olympus, 25-105) coated with Vitronectin (Gibco, A14700) in DPBS. iPSCs were dissociated and passaged using EDTA (Invitrogen, AM9260G) in DPBS. This work was approved by UCSF GESCR Committee.

Cortical-like neuronal induction

Cortical-like iN were generated as previously described (Fernando-pulle et al., 2018). Briefly, iPSCs (WTC11) were expanded, dissociated, and replated on 10 µg/mL Matrigel (Corning, 354234) coated plates. Cells were grown in specialized iNeuron induction media

(DMEM-F12 + Glutamax; Gibco, 10565-018), N-2 supplement (Gibco, 17502-048), MEM-NEAA (Gibco, 11140-050) containing doxycycline (Sigma, D3072) for approximately 72 h, with media changed every approximately 24 h. Cells were then dissociated using Accutase (Gibco, A1110501) and frozen in media +10% DMSO (Sigma, D8418) at high density to maximize cell viability.

Statistical analyses

Statistical analyses were done using Prism 9.0 (GraphPad). If normally distributed, two-tailed unpaired Student's t test was performed. If normally distributed, a one-way ANOVA was performed. A p value of less than 0.05 was considered significant. If non-normally distributed, a Mann-Whitney U-test was performed. A p value of less than 0.05 was considered significant. Using DESeq2, Wald tests were performed to evaluate genes for differential expression between conditions. The false discovery rate multiple testing correction method was then used for adjusted p values.

SUPPLEMENTAL INFORMATION

Supplemental information can be found online at <https://doi.org/10.1016/j.stemcr.2023.01.012>.

AUTHOR CONTRIBUTIONS

M.dM., M.Koontz, and E.M.U. designed experiments. M.dM., M.Koontz, E.M., N.S., A.R., Y.K., S.L.G., N.M.D., and K.L. performed experiments and/or analyzed data. Y.M. generated the *GRN*^{-/-} iPSC lines. M.dM., E.M.U., E.M., H.L., and K.S. conceived the hypothesis. E.M., J.R.K., M.Kurnellas, M.Kampmann, M.E.W., E.J.H., and E.M.U. provided resources. M.dM., M.Koontz, E.M., and E.M.U. wrote the manuscript. All authors reviewed and approved the manuscript.

ACKNOWLEDGMENTS

We thank Arnab Ghosh and Efy Hernandez of the UCSF Genomics Co-Lab for the RNA-seq Library preparation and raw analysis. We would also like to thank Su Ling Wang for her contribution on the figure graphics. Furthermore, we thank Bruce Conklin for support and advice. This study has been supported by NIH/NIA R01 AG057528 (M. Kampmann), AG062422-01 (H.L.) 2 P30 EY02162-39 (E.M.U.) and R03AG063157 (E.M.U.), R44NS124457 (M.dM., E.M.U.), the post-doctoral fellowship from the American Federation for Aging Research (AFAR) and Glenn Foundation for Medical Research (E.M.), the Reboot Grant from the AFAR (E.M.). This study was funded in part by the UCSF Vision Core shared resource of the NIH/NEI P30 EY002162, and by an unrestricted grant from Research to Prevent Blindness, New York, NY (Y.K., E.M.U.). This work was also partially supported by Synapticure Inc and Alector.

CONFLICT OF INTERESTS

M.dM. and M.Koontz are full-time employees and equity holders of Synapticure Inc. E.M.U. is an equity holder of Synapticure Inc. M. Kampmann is an inventor on U.S. Patent 11,254,933 related to CRISPRi and CRISPRa screening, serves on the Scientific Advisory Boards of Engine Biosciences, Casma Therapeutics, Cajal



Neuroscience, and Alector, and is an advisor to Modulo Bio and Recursion Therapeutics. J.R.K. is a shareholder of Faze Medicines and QurAlis, and is an author on patent that describes surfaces for the long-term culture of pluripotent cells (U.S. patent 8,648,170) as well as a patent application that describes methods and compositions for restoring STMN2 levels (U.S. patent application 20,220,133,848). M.Kurnellas is a full-time employee and has equity interest in Alector, Inc. N.M.Dräger is a full time employee at Modulo Bio, Inc. All other authors declare no conflict of interest.

Received: November 29, 2021

Revised: January 24, 2023

Accepted: January 25, 2023

Published: February 23, 2023

REFERENCES

- Ahmed, Z., Sheng, H., Xu, Y., Lin, W.-L., Innes, A.E., Gass, J., Yu, X., Hou, H., Chiba, S., Yamanouchi, K., et al. (2010). Accelerated lipofuscinosis and ubiquitination in granulin knockout mice suggest a role for progranulin in successful aging. *Am. J. Pathol.* *177*, 311–324. <https://doi.org/10.2353/ajpath.2010.090915>.
- Akiyama, T., Koike, Y., Petrucelli, L., and Gitler, A.D. (2022). Cracking the cryptic code in amyotrophic lateral sclerosis and frontotemporal dementia: towards therapeutic targets and biomarkers. *Clin. Transl. Med.* *12*. <https://doi.org/10.1002/ctm2.818>.
- Almeida, S., Zhang, Z., Coppola, G., Mao, W., Futai, K., Karydas, A., Geschwind, M.D., Tartaglia, M.C., Gao, F., Gianni, D., et al. (2012). Induced pluripotent stem cell models of progranulin-deficient frontotemporal dementia uncover specific reversible neuronal defects. *Cell Rep.* *2*, 789–798. <https://doi.org/10.1016/j.celrep.2012.09.007>.
- Baker, M., Mackenzie, I.R., Pickering-Brown, S.M., Gass, J., Rademakers, R., Lindholm, C., Snowden, J., Adamson, J., Sadovnick, A.D., Rollinson, S., et al. (2006). Mutations in progranulin cause tau-negative frontotemporal dementia linked to chromosome 17. *Nature*. <https://doi.org/10.1038/nature05016>.
- Bellenguez, C., Grenier-Boley, B., and Lambert, J.-C. (2020). Genetics of Alzheimer's disease: where we are, and where we are going. *Curr. Opin. Neurobiol.* *61*, 40–48. <https://doi.org/10.1016/j.conb.2019.11.024>.
- Blanchard, J.W., Bula, M., Davila-Velderrain, J., Akay, L.A., Zhu, L., Frank, A., Victor, M.B., Bonner, J.M., Mathys, H., Lin, Y.-T., et al. (2021). Author Correction: reconstruction of the human blood-brain barrier in vitro reveals a pathogenic mechanism of APOE4 in pericytes. *Nat. Med.* *27*, 356. <https://doi.org/10.1038/s41591-021-01250-8>.
- Bossolasco, P., Cimini, S., Maderna, E., Bardelli, D., Canafoglia, L., Cavallaro, T., Ricci, M., Silani, V., Marucci, G., and Rossi, G. (2022). GRN^{-/-} iPSC-derived cortical neurons recapitulate the pathological findings of both frontotemporal lobar degeneration and neuronal ceroidlipofuscinosis. *Neurobiol. Dis.*, 105891. <https://doi.org/10.1016/j.nbd.2022.105891>.
- Brown, A.-L., Wilkins, O.G., Keuss, M.J., Hill, S.E., Zanolletto, M., Lee, W.C., Bampton, A., Lee, F.C.Y., Masino, L., Qi, Y.A., et al. (2022). TDP-43 loss and ALS-risk SNPs drive mis-splicing and depletion of UNC13A. *Nature* *13*, 16. <https://doi.org/10.1038/s41586-022-04436-3>.
- Buratti, E. (2020). Targeting TDP-43 proteinopathy with drugs and drug-like small molecules. *Br. J. Pharmacol.* <https://doi.org/10.1111/bph.15148>.
- Burrell, J.R., Halliday, G.M., Kril, J.J., Ittner, L.M., Götz, J., Kiernan, M.C., and Hodges, J.R. (2016). The frontotemporal dementia-motor neuron disease continuum. *Lancet*. [https://doi.org/10.1016/S0140-6736\(15\)60684-5](https://doi.org/10.1016/S0140-6736(15)60684-5).
- Chiò, A., Logroscino, G., Traynor, B.J., Collins, J., Simeone, J.C., Goldstein, L.A., and White, L.A. (2013). Global epidemiology of amyotrophic lateral sclerosis: a systematic review of the published literature. *Neuroepidemiology* *41*, 118–130. <https://doi.org/10.1159/000351153>.
- Chung, W.-S., Clarke, L.E., Wang, G.X., Stafford, B.K., Sher, A., Chakraborty, C., Joung, J., Foo, L.C., Thompson, A., Chen, C., et al. (2013). Astrocytes mediate synapse elimination through MEGF10 and MERTK pathways. *Nature* *504*, 394–400. <https://doi.org/10.1038/nature12776>.
- Coyne, A.N., Baskerville, V., Zaepfel, B.L., Dickson, D.W., Rigo, F., Bennett, F., Patrick Lusk, C., and Rothstein, J.D. (2021). Nuclear accumulation of CHMP7 initiates nuclear pore complex injury and subsequent TDP-43 dysfunction in sporadic and familial ALS. *Sci. Transl. Med.* *13*. <https://doi.org/10.1126/scitranslmed.abe1923>.
- Cruts, M., Gijselinck, I., van der Zee, J., Engelborghs, S., Wils, H., Pirici, D., Rademakers, R., Vandenberghe, R., Dermaut, B., Martin, J.J., et al. (2006). Null mutations in progranulin cause ubiquitin-positive frontotemporal dementia linked to chromosome 17q21. *Nature*. <https://doi.org/10.1038/nature05017>.
- Desai, M.K., Mastrangelo, M.A., Ryan, D.A., Sudol, K.L., Narrow, W.C., and Bowers, W.J. (2010). Early oligodendrocyte/myelin pathology in Alzheimer's disease mice constitutes a novel therapeutic target. *Am. J. Pathol.* *177*, 1422–1435. <https://doi.org/10.2353/ajpath.2010.100087>.
- Dräger, N.M., Sattler, S.M., Huang, C.T.-L., Teter, O.M., Leng, K., Hashemi, S.H., Hong, J., Aviles, G., Clelland, C.D., Zhan, L., et al. (2022). A CRISPRi/a platform in human iPSC-derived microglia uncovers regulators of disease states. *Nat. Neurosci.* <https://doi.org/10.1038/s41593-022-01131-4>.
- Fernandopulle, M.S., Prestil, R., Grunseich, C., Wang, C., Gan, L., and Michael, E. (2018). Transcription-factor mediated differentiation of human iPSCs into neurons Running Title Rapid differentiation of iPSCs into neurons. *Current Protocols in Cell Biology*. <https://doi.org/10.1002/cpcb.51>.
- Guan, Z., Chen, Z., Fu, S., Dai, L., and Shen, Y. (2020). Progranulin administration attenuates β -amyloid deposition in the Hippocampus of 5xFAD mice through modulating BACE1 expression and microglial phagocytosis. *Front. Cell. Neurosci.* *14*. <https://doi.org/10.3389/fncel.2020.00260>.
- Hansen, D.v., Hanson, J.E., and Sheng, M. (2018). Microglia in Alzheimer's disease. In *JCB (J. Cell Biol.)*, 217 (Rockefeller University Press), pp. 459–472. <https://doi.org/10.1083/jcb.201709069>.



- Huang, J., Li, C., and Shang, H. (2022). Astrocytes in neurodegeneration: inspiration from genetics. *Front. Neurosci.* *16*. <https://doi.org/10.3389/fnins.2022.882316>.
- Kelley, K.W., Nakao-Inoue, H., Molofsky, A.v., and Oldham, M.C. (2018). Variation among intact tissue samples reveals the core transcriptional features of human CNS cell classes. *Nat. Neurosci.* *21*, 1171–1184. <https://doi.org/10.1038/s41593-018-0216-z>.
- Klim, J.R., Williams, L.A., Limone, F., San Juan, I.G., Davis-Dusenbery, B.N., Mordes, D.A., Butberry, A., Steinbaugh, M.J., Gamage, K.K., Kirchner, R., et al. (2019). ALS-implicated protein TDP-43 sustains levels of STMN2, a mediator of motor neuron growth and repair. *Neuron* *103*, 43–54. <https://doi.org/10.1016/j.neuron.2019.04.019>.
- Knopman, D.S., and Roberts, R.O. (2011). Estimating the number of persons with frontotemporal lobar degeneration in the US population. *J. Mol. Neurosci.* *45*, 330–335. <https://doi.org/10.1007/s12031-011-9538-y>.
- Krencik, R., Hokanson, K.C., Narayan, A.R., Dvornik, J., Rooney, G.E., Rauen, K.A., Weiss, L.A., Rowitch, D.H., and Ullian, E.M. (2015). Dysregulation of astrocyte extracellular signaling in Costello syndrome. *Sci. Transl. Med.* *7*, 1–12. <https://doi.org/10.1126/scitranslmed.aaa5645>.
- Krencik, R., Seo, K., van Asperen, J.v., Basu, N., Cvetkovic, C., Barlas, S., Chen, R., Ludwig, C., Wang, C., Ward, M.E., et al. (2017). Systematic three-dimensional coculture rapidly recapitulates interactions between human neurons and astrocytes. *Stem Cell Rep.* *9*, 1745–1753. <https://doi.org/10.1016/j.stemcr.2017.10.026>.
- Krencik, R., and Zhang, S.-C. (2011). Directed differentiation of functional astroglial subtypes from human pluripotent stem cells. *Nat. Protoc.* *6*, 1710–1717. <https://doi.org/10.1038/nprot.2011.405>.
- Kumar, A., D'Souza, S.S., Moskvina, O.V., Toh, H., Wang, B., Zhang, J., Swanson, S., Guo, L.-W., Thomson, J.A., and Slukvin, I.I. (2017). Specification and diversification of pericytes and smooth muscle cells from mesenchymal stem cells. *Cell Rep.* *19*, 1902–1916. <https://doi.org/10.1016/j.celrep.2017.05.019>.
- Lee, E., and Chung, W.-S. (2019). Glial control of synapse number in healthy and diseased brain. *Front. Cell. Neurosci.* *13*, 42. <https://doi.org/10.3389/fncel.2019.00042>.
- Lee, and Huang, E.J. (2017). Modeling ALS and FTD with iPSC-derived neurons. In *Brain Res.*, 1656 (Elsevier B.V), pp. 88–97. <https://doi.org/10.1016/j.brainres.2015.10.003>.
- Leng, K., Rose, I.V.L., Kim, H., Xia, W., Romero-Fernandez, W., Rooney, B., Koontz, M., Li, E., Ao, Y., Wang, S., et al. (2022). CRISPRi screens in human iPSC-derived astrocytes elucidate regulators of distinct inflammatory reactive states. *Nat. Neurosci.* *25*, 1528–1542. <https://doi.org/10.1038/s41593-022-01180-9>.
- Liddel, S.A., Guttenplan, K.A., Clarke, L.E., Bennett, F.C., Bohlen, C.J., Schirmer, L., Bennett, M.L., Münch, A.E., Chung, W.S., Peterson, T.C., et al. (2017). Neurotoxic reactive astrocytes are induced by activated microglia. *Nature*. <https://doi.org/10.1038/nature21029>.
- Ling, S.-C., Polymenidou, M., and Cleveland, D.W. (2013). Converging mechanisms in ALS and FTD: disrupted RNA and protein homeostasis. *Neuron* *79*, 416–438. <https://doi.org/10.1016/j.neuron.2013.07.033>.
- Liu, S.J., Malatesta, M., Lien, B.V., Saha, P., Thombare, S.S., Hong, S.J., Pedraza, L., Koontz, M., Seo, K., Horlbeck, M.A., et al. (2020). CRISPRi-based radiation modifier screen identifies long non-coding RNA therapeutic targets in glioma. *Genome Biol.* *21*, 83. <https://doi.org/10.1186/s13059-020-01995-4>.
- Logan, T., Simon, M.J., Rana, A., Cherf, G.M., Srivastava, A., Davis, S.S., Low, R.L.Y., Chiu, C.L., Fang, M., Huang, F., et al. (2021). Rescue of a lysosomal storage disorder caused by Grn loss of function with a brain penetrant progranulin biologic. *Cell* *184*, 4651–4668.e25. <https://doi.org/10.1016/j.cell.2021.08.002>.
- Lui, H., Zhang, J., Makinson, S.R., Cahill, M.K., Kelley, K.W., Huang, H.Y., Shang, Y., Oldham, M.C., Martens, L.H., Gao, F., et al. (2016). Progranulin deficiency promotes circuit-specific synaptic pruning by microglia via complement activation. *Cell* *165*, 921–935. <https://doi.org/10.1016/j.cell.2016.04.001>.
- Mackenzie, I.R.A. (2007). The neuropathology and clinical phenotype of FTD with progranulin mutations. In *Acta Neuropathologica*. <https://doi.org/10.1007/s00401-007-0223-8>.
- Mantle, J.L., and Lee, K.H. (2018). A differentiating neural stem cell-derived astrocytic population mitigates the inflammatory effects of TNF- α and IL-6 in an iPSC-based blood-brain barrier model. *Neurobiol. Dis.* *119*, 113–120. <https://doi.org/10.1016/j.nbd.2018.07.030>.
- Melamed, Z., López-Erauskin, J., Baughn, M.W., Zhang, O., Drenner, K., Sun, Y., Freyermuth, F., McMahon, M.A., Beccari, M.S., Artates, J.W., et al. (2019). Premature polyadenylation-mediated loss of stathmin-2 is a hallmark of TDP-43-dependent neurodegeneration. *Nat. Neurosci.* *22*, 180–190. <https://doi.org/10.1038/s41593-018-0293-z>.
- Miyaoka, Y., Chan, A.H., Judge, L.M., Yoo, J., Huang, M., Nguyen, T.D., Lizarraga, P.P., So, P.-L., and Conklin, B.R. (2014). Isolation of single-base genome-edited human iPSC cells without antibiotic selection. *Nat. Methods* *11*, 291–293. <https://doi.org/10.1038/nmeth.2840>.
- Nelson, P.T., Brayne, C., Flanagan, M.E., Abner, E.L., Agrawal, S., Attems, J., Castellani, R.J., Corrada, M.M., Cykowski, M.D., Di, J., et al. (2022). Frequency of LATE neuropathologic change across the spectrum of Alzheimer's disease neuropathology: combined data from 13 community-based or population-based autopsy cohorts. *Acta Neuropathol.* <https://doi.org/10.1007/s00401-022-02444-1>.
- Nelson, P.T., Dickson, D.W., Trojanowski, J.Q., Jack, C.R., Boyle, P.A., Arfanakis, K., Rademakers, R., Alafuzoff, I., Attems, J., Brayne, C., et al. (2019). Limbic-predominant age-related TDP-43 encephalopathy (LATE): consensus working group report. *Brain* *142*, 1503–1527. <https://doi.org/10.1093/brain/awz099>.
- Neumann, M., Sampathu, D.M., Kwong, L.K., Truax, A.C., Micney, M.C., Chou, T.T., Bruce, J., Schuck, T., Grossman, M., Clark, C.M., et al. (2006). Ubiquitinated TDP-43 in frontotemporal lobar degeneration and amyotrophic lateral sclerosis. *Science (New York, N.Y.)* *314*, 130–133. <https://doi.org/10.1126/science.1134108>.
- Palomo, V., Tosat-Bitrian, C., Nozal, V., Nagaraj, S., Martin-Requero, A., and Martinez, A. (2019). TDP-43: a key therapeutic target beyond amyotrophic lateral sclerosis. *ACS Chem. Neurosci.* *10*, 1183–1196. <https://doi.org/10.1021/acschemneuro.9b00026>.



- Petoukhov, E., Fernando, S., Mills, F., Shivji, F., Hunter, D., Krieger, C., Silverman, M.A., and Bamji, S.X. (2013). Activity-dependent secretion of progranulin from synapses. *J. Cell Sci.* *126*, 5412–5421. <https://doi.org/10.1242/jcs.132076>.
- Prudencio, M., Humphrey, J., Pickles, S., Brown, A.-L., Hill, S.E., Kachergus, J., Shi, J., Heckman, M., Spiegel, M., Cook, C., et al. (2020). Truncated stathmin-2 is a marker of TDP-43 pathology in frontotemporal dementia. *J. Clin. Invest.* <https://doi.org/10.1172/jci139741>.
- Quek, H., Cuní-López, C., Stewart, R., Colletti, T., Notaro, A., Nguyen, T.H., Sun, Y., Guo, C.C., Lupton, M.K., Roberts, T.L., et al. (2022). ALS monocyte-derived microglia-like cells reveal cytoplasmic TDP-43 accumulation, DNA damage, and cell-specific impairment of phagocytosis associated with disease progression. *J. Neuroinflammation* *19*. <https://doi.org/10.1186/s12974-022-02421-1>.
- Rhinn, H., Tatton, N., McCaughey, S., Kurnellas, M., and Rosenthal, A. (2022). Progranulin as a therapeutic target in neurodegenerative diseases. In *Trends in Pharmacological Sciences* (Elsevier Ltd). <https://doi.org/10.1016/j.tips.2021.11.015>.
- Rosen, E.Y., Wexler, E.M., Versano, R., Coppola, G., Gao, F., Winden, K.D., Oldham, M.C., Martens, L.H., Zhou, P., Farese, R.V., Jr., and Geschwind, D.H. (2011). Functional genomic analyses identify pathways dysregulated by progranulin deficiency, implicating wnt signaling. *Neuron* *71*, 1030–1042. <https://doi.org/10.1016/j.neuron.2011.07.021>.
- Seelaar, H., Kamphorst, W., Rosso, S.M., Azmani, A., Masdjedi, R., de Koning, I., Maat-Kievit, J.A., Anar, B., Kaat, L.D., Breedveld, G.J., et al. (2008). Distinct genetic forms of frontotemporal dementia. *Neurology* *71*, 1220. <https://doi.org/10.1212/01.wnl.0000319702.37497.72>.
- Taha, D.M., Clarke, B.E., Hall, C.E., Tyzack, G.E., Ziff, O.J., Green-smith, L., Kalmar, B., Ahmed, M., Alam, A., Thelin, E.P., et al. (2022). Astrocytes display cell autonomous and diverse early reactive states in familial amyotrophic lateral sclerosis. *Brain*. <https://doi.org/10.1093/brain/awab328>.
- Tapia, L., Milnerwood, A., Guo, A., Mills, F., Yoshida, E., Vasuta, C., Mackenzie, I.R., Raymond, L., Cynader, M., Jia, W., and Bamji, S.X. (2011). Progranulin deficiency decreases gross neural connectivity but enhances transmission at individual synapses. *J. Neurosci.* *31*, 11126. <https://doi.org/10.1523/JNEUROSCI.6244-10.2011>.
- Uesaka, N., Abe, M., Konno, K., Yamazaki, M., Sakoori, K., Watanabe, T., Kao, T.-H., Mikuni, T., Watanabe, M., Sakimura, K., and Kano, M. (2018). Retrograde signaling from progranulin to Sort1 counteracts synapse elimination in the developing cerebellum. *Neuron* *97*, 796–805.e5. <https://doi.org/10.1016/j.neuron.2018.01.018>.
- Verkhatsky, A., Olabarria, M., Noristani, H.N., Yeh, C.-Y., and Rodriguez, J.J. (2010). Astrocytes in Alzheimer's disease. *Neurotherapeutics* *7*, 399–412. <https://doi.org/10.1016/j.nurt.2010.05.017>.
- Viswanathan, J., Mäkinen, P., Helisalmi, S., Haapasalo, A., Soininen, H., and Hiltunen, M. (2009). An association study between granulin gene polymorphisms and Alzheimer's disease in Finnish population. *Am. J. Med. Genet. Part B: Neuropsychiatric Genetics* *150B5*, 747–750. <https://doi.org/10.1002/ajmg.b.30889>.
- Wang, C., Ward, M.E., Chen, R., Liu, K., Tracy, T.E., Chen, X., Xie, M., Sohn, P.D., Ludwig, C., Meyer-Franke, A., et al. (2017). Scalable production of iPSC-derived human neurons to identify tau-lowering compounds by high-content screening. *Stem Cell Rep.* *9*, 1221–1233. <https://doi.org/10.1016/j.stemcr.2017.08.019>.
- Wang, L., Chen, J., Hu, Y., Liao, A., Zheng, W., Wang, X., Lan, J., Shen, J., Wang, S., Yang, F., et al. (2022). Progranulin improves neural development via the PI3K/Akt/GSK-3 β pathway in the cerebellum of a VPA-induced rat model of ASD. *Transl. Psychiatry* *12*, 114. <https://doi.org/10.1038/s41398-022-01875-4>.
- Ward, M.E., Taubes, A., Chen, R., Miller, B.L., Sephton, C.F., Gelfand, J.M., Minami, S., Boscardin, J., Martens, L.H., Seeley, W.W., et al. (2014). Early retinal neurodegeneration and impaired Ran-mediated nuclear import of TDP-43 in progranulin-deficient FTLD. *J. Exp. Med.* *211*, 1937–1945. <https://doi.org/10.1084/jem.20140214>.
- Zhang, J., Velmeshev, D., Hashimoto, K., Huang, Y.H., Hofmann, J.W., Shi, X., Chen, J., Leidal, A.M., Dishart, J.G., Cahill, M.K., et al. (2020). Neurotoxic microglia promote TDP-43 proteinopathy in progranulin deficiency. *Nature*. <https://doi.org/10.1038/s41586-020-2709-7>.
- Zhang, Y., Chen, K., Sloan, S.A., Bennett, M.L., Scholze, A.R., O'Keeffe, S., Phatnani, H.P., Guarnieri, P., Caneda, C., Ruderisch, N., et al. (2014). An rna-sequencing transcriptome and splicing database of glia, neurons, and vascular cells of the cerebral cortex. *The J. of Neuroscience* *34*, 11929. <https://doi.org/10.1523/JNEUROSCI.1860-14.2014>.
- Zhang, Y., Sloan, S.A., Clarke, L.E., Caneda, C., Plaza, C.A., Blumenthal, P.D., Vogel, H., Steinberg, G.K., Edwards, M.S.B., Li, G., et al. (2016). Purification and characterization of progenitor and mature human astrocytes reveals transcriptional and functional differences with mouse. *Neuron* *89*, 37–53. <https://doi.org/10.1016/j.neuron.2015.11.013>.

Stem Cell Reports, Volume 18

Supplemental Information

Granulin loss of function in human mature brain organoids implicates astrocytes in TDP-43 pathology

Martina de Majo, Mark Koontz, Elise Marsan, Nir Salinas, Arren Ramsey, Yien-Ming Kuo, Kyounghee Seo, Huinan Li, Nina Dräger, Kun Leng, Santiago L. Gonzales, Michael Kurnellas, Yuichiro Miyaoka, Joseph R. Klim, Martin Kampmann, Michael E. Ward, Eric J. Huang, and Erik M. Ullian

Supplementary Material

2D and 3D cell culture

iNeurons Validation: iNeurons were matured in 2D monoculture for four weeks by thawing and plating previously induced, harvested, and frozen iNeurons onto PDL (Sigma, P6407-5mg) coated six-well plates. iNeuron cultures were fed with BrainPhys Complete media (BrainPhys basal (StemCell Tech, 05790), Laminin (Gibco, 23017-015), NT3 (Peprotech, 450-03), BDNF (Peprotech, 450-02), N2 (Gibco, 17502-048), B27 -Vit.A (Gibco, 12587-010), HEPES (Gibco, 15630-106)) and maintained with ~2mls/well and a 50% media change every 72 hrs.

iAstrocyte validation: On approximately day 120, cultures were initially validated as astrocyte progenitor cells using ICC to confirm post-mitotic behavior, stellate morphology and canonical astrocyte gene expression (**FigS2 A-C**). On day 0 of ICC validation, a small number of spheroids were triturated into a single cell suspension and plated on Matrigel coated glass cover-slips at ~10k cells/cm² using ASM plus CNTF and BMP4 (Peprotech, 450-13 & 120-05ET). Media was changed every 48 hours. On day 7, cultures were fixed with 4% PFA and processed for ICC validation.

2D co-cultures: iNeurons and iAstrocytes were plated together at 1:1 ratio on Matrigel coated 24 well plates at a collective density of ~1x10⁶ cells/well. Cells were maintained with BrainPhys Complete media at ~1ml/well with a 50% media change every 72 hrs.

3D co-cultures: iNeurons and iAstrocytes were maintained, validated, and cryo-preserved in order to maximize consistency and repeatability across multiple iterations of various experiments described herein. 3D mbOrgs co-cultures were prepared by thawing or dissociating constitutive cell types in single cell suspension. Cell types were then combined at specified ratios (1:1, iAst:iN) prior to being aliquoted into round-bottom plates. Plates were briefly centrifuged and left undisturbed for ~24 hours, allowing cells to coalesce into self-assembled spheroids. mbOrgs were maintained with a partial media change every 72 hours using BrainPhys Complete media.

Cortical-like astrocyte induction

Cortical-like iAstrocytes (iA) were generated as previously described (Krencik & Zhang, 2011). Human induced pluripotent stem cells (WTC11) were grown on vitronectin coated tissue culture plates using Essential 8 media. On day 0 of differentiation, iPSCs were dissociated into small aggregates averaging 50µm in diameter and transferred untreated tissue culture flasks with Neurosphere Induction Media (NSIM) (DMEM-F12/Neurobasal-A at 1:1 (Gibco, 10565-018: 108888-022)), N2 Supplement (Gibco, 17502-048), B27 -Vit.A Supplement (Gibco, 12587-010), MEM-NEAA (Gibco, 11140-050) plus SMAD inhibitors SB431542 (Stemcell Tech, 72234) and DMH1 (Tocris, 73634). Neurosphere induction media (NIM) plus SMAD inhibitors were changed every 48 hours. On day 7, once embryoid bodies began to show rosette clusters indicating early neuroepithelia morphological hallmarks, spheroids were transferred to Matrigel (Corning, 354230) coated tissue culture plates with NIM and SMAD inhibitors were removed. Media was changed every 24 hours until spheroids had sufficiently attached, and each spheroid exposed the rosette clusters within. On day 14, rosette clusters were mechanically removed and transferred to tissue culture flasks with NIM plus FGFb (Peprotech, 100-18B). Media was changed every 72 hours. On day 20, spheroids were triturated into a single cell suspension and transferred to a new untreated cell culture flask with astrocyte media (ASM) (DMEM-F12 (Gibco, 10565-018), N2 Supplement (Gibco, 17502-048), B27 -Vit.A Supplement (Gibco, 12587-010), Heparin (Stemcell Tech, 07980)) plus Y27632 (Tocris, 1254). From Day 28 to 180, spheroid aggregates were maintained in suspension with ASM plus EGF and FGFb (Peprotech, 100-15 & 100-18B) with media changes every 4-5 days. Spheroid aggregates were triturated every 7-10 days and transferred to new untreated tissue culture flasks.

Rescue experiment

Cells were plated as described above including an extra set of *GRN*^{-/-} co-cultures which were treated with PGRN at 1µg/ml (Adipogen, AG-40A-0188Y). Media was partially changed and treatment replenished every 72 hours. Cells were then processed for RNA extraction or immunocytochemistry as described below.

Western blot

mbOrg or 2D cultures were lysed in RIPA buffer (Thermo Fisher Scientific Cat#PI89900) complemented with Phosphatase and Protease inhibitors (Thermo Fisher Scientific Cat#1862495 and 1862209) according to manufacturer's indications. Lysates were sonicated (QSonica, 55W, 110V Cat#Q55-110) for 10s/sample on ice and protein concentration was determined using Pierce BCA protein assay kit following manufacturer's instruction (Thermo Fisher Scientific cat#23227). 20µg to 30 µg of total protein from each lysate was combined with loading buffer (4X, Thermo Fisher Scientific, Cat#84788) and beta mercaptoethanol (0.05 M, BioRad Laboratories Cat#1610710) and loaded into a NuPAGE 4%–12% or 10% Bis-Tris Gel (Invitrogen, Cat# NP0336BOX, NP0301BOX) alongside a protein ladder (Thermo Fisher Scientific Cat#26619) to determine protein size. The gels were run in MOPS (Thermo Fisher Scientific Cat# NP0001) or MES (Invitrogen Cat#NP0002) buffer depending on the desired protein separation. Subsequently, the gel was transferred onto a nitrocellulose membrane using Trans Blot Sd Semi-Dry Transfer Cell (BioRad Cat#1703940) according to the manufacturer's instructions. After transfer, the membrane was stained with PonceauS, washed and blocked in 5% milk in PBS-T (PBS with 0.02% tween) or 10% BSA TBST-T (TBS + 0.02 tween), followed by overnight incubation with primary antibodies in 1% Milk or BSA at 4C (Table1). After incubation, the membrane was washed three times with PBS-T or TBS-T and then incubated with HRP conjugated secondary antibodies (Thermo Scientific Pierce Goat anti rabbit Cat#32260 or Goat anti mouse Cat#32230) at room temperature for 1hr. The membrane was then washed 3 times with PBS-T, incubated for two minutes with Pierce ECL western blotting substrate (Thermo Fisher Cat# 32106) and imaged at ChemiDoc (BioRad). Digital images were processed and analyzed using the image analysis software, ImageLab (BioRad).

Table 1. Primary antibodies used for western blot

Target	Vendor and Cat#	Concentration
GAPDH	Sigma-Aldrich, Cat# G8795	1:3000
PGRN	ThermoFisher, cat# 40-3400	1:250
TDP-43	Proteintech Cat#66734-1-1g	1:500
Phospho-TDP43 (Ser409/410)	Proteintech Cat#80007-1-RR	1:500
SYN1	Synaptic Systems Cat#101-004	1:300
PSD95	Abcam Cat#Ab18258	1:500

3D Organoid sample processing and cryosectioning for ICC

Samples were fixed in 4% PFA for ~25 minutes and washed three times with DPBS. Samples were then incubated overnight at 4°C in DPBS plus 30% sucrose and transitioned to a 1:1 solution of OCT & DPBS containing a final concentration of 30% sucrose. Samples were then incubated in OCT at RT for ~15 minutes prior to being embedded in OCT and frozen. OCT embedded samples were then cryosectioned at 20µm intervals using a Leica cryostat prior to applying the ICC protocol detailed below.

Immunocytochemistry

For 2D cultures, cells were gently washed in DPBS and fixed in 4% PFA (EMS; 50-980-487). Samples were washed three times in DPBS and incubated with blocking buffer (Glycine 0.1M, 5% goat/donkey serum, 1% BSA, 0.25% TritonX, 100mM glycine in DPBS) for one hour at room temperature. Samples were then incubated overnight with primary antibody (Table 2) at the appropriate concentration in primary blocking buffer (5% goat/donkey serum, 1%BSA, 0.25% triton X-100, 100nM glycine in DPBS) at 4C overnight, washed three times in DPBS and incubated with secondary antibodies (Table 3) diluted in secondary blocking buffer (10% BSA in DPBS) at room temperature for 1h. Samples were washed three times in DPBS and incubated with DAPI (Sigma-Aldrich Inc Cat#D9542-5MG) for 1 min at RT and washed twice in DPBS. If on coverslips, samples were mounted on microscope slides (Fisher Scientific Cat#1255015) using ProLong Gold (Invitrogen Cat#P36934) and dried at room temperature overnight. Sections were imaged at LSM900 confocal microscope (Zeiss) or Fluorescent microscopy images were acquired using a Revolve microscope (Echo Laboratories, San Diego, CA, USA). Images were analyzed using ImageJ(FIJI) (Schindelin et al., 2012).

For 3D cultures, slices were stained as described above. Briefly, we used a hydrophobic pen to delimitate the area of staining. We then washed with PBS to clean the excess OCT and start with the protocol described above. The PGRN antibody staining protocol included an antigen retrieval treatment by incubating tissue sections in 10 mM sodium citrate (pH 6.0) at 90°C for 10 minutes before the incubation in the blocking solution. For all 3D slices, labeling was done at room temperature, but samples were treated otherwise the same as 2D cultures.

Table 2. Primary antibodies used for ICC

Target	Vendor and Cat#	Concentration
NFIA	Sigma Cat#HPA008884	1:200 (2D) 1:400 (3D)
TUJ1	Millipore Cat#AB9354	1:200
AQP4	Sigma Cat#HPA014784	1:500
CD44	BD bioscience Cat#559046	1:200
GFAP δ	Milipore Cat#AB9598	1:500
TDP-43	Proteintech Cat#66734-1-1g	1:500
Phospho-TDP43 (Ser409/410)	Proteintech Cat#22309-1-AP	1:500
PGRN	R&D Sys. Cat#AF2557	1:100
PGRN	R&D Sys. Cat#AF2420	1:2000
MAP2	Abcam Cat#ab5392	1:500
PSD 95	Abcam Cat#ab13552	1:200
SYP	Synaptic Sys. Cat#101004	1:200

Table 3. Secondary antibodies used for ICC

Target	Vendor and Cat#	Concentration
Goat-Anti-Mouse Alexa 568	Thermofisher Scientific, A11004	1:500

Goat-Anti-Chicken Alexa 647	Thermofisher Scientific, A21449	
Goat-Anti-Rabbit Alexa 488	Thermofisher Scientific, A11008	
Donkey-Anti-Mouse Alexa 647	Thermofisher Scientific, A21202	
Donkey-Anti-Goat Alexa 594	Thermofisher Scientific, A11058	

IMARIS reconstruction

IMARISx64 was used to create a 3D reconstruction of the original z-stack using the different color channels.

Extranuclear TDP-43 analysis

TDP-43 quantifications were performed on FIJI. The DAPI channel and TDP-43 channel were each thresholded. Then, the image calculator was used to subtract the DAPI channel from the TDP-43 channel. Analyze Particles (0 μm^2 – infinity) was used on the resulting image to quantify the number and area of the non-nuclear TDP-43. The DAPI channel was then used to create a selection that was restored on the TDP-43 channel, such that the nuclear TDP-43 was highlighted, and the intensity could be measured in that region.

RNA isolation for bulk RNAseq and RT-PCR

RNA extraction was performed using the Trizol/phenol-Chloroform method (Sigma, T9424) as previously described (Krencik et al., 2015) and according to manufacturer specifications. Each sample contained ~50 mbOrgs, totaling $\sim 2.5 \times 10^6$ of cells per sample. The extracted RNA was used as a template for the synthesis of complementary DNA (cDNA) through reverse transcription, using iScript(tm) cDNA Synthesis Kit (Bio-Rad Cat#1708891) according to the manufacturer's protocol.

Quantitative PCR

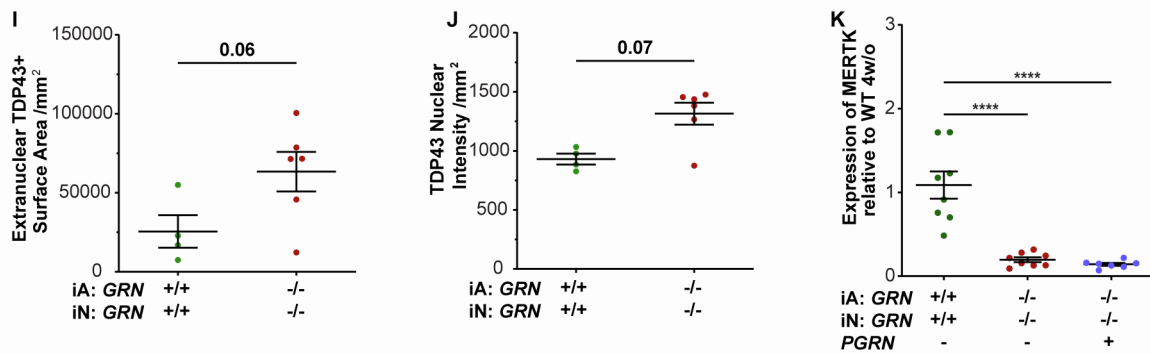
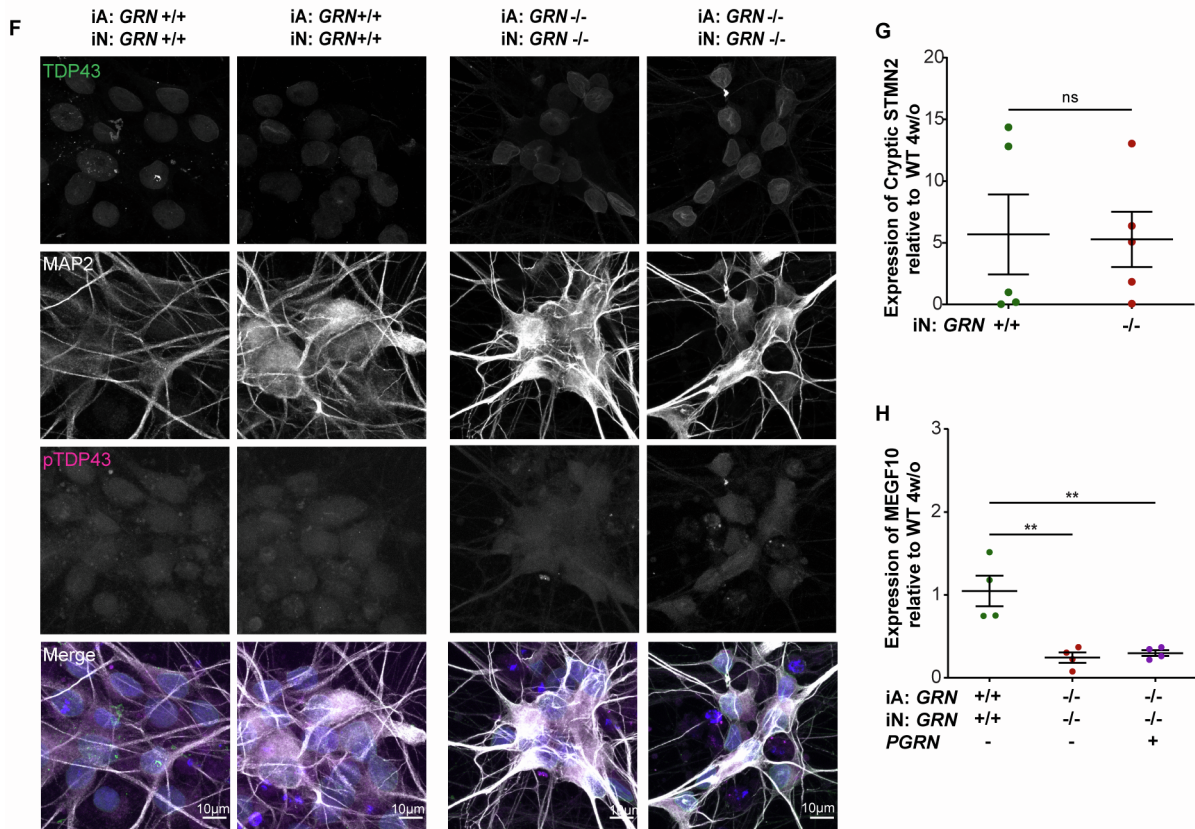
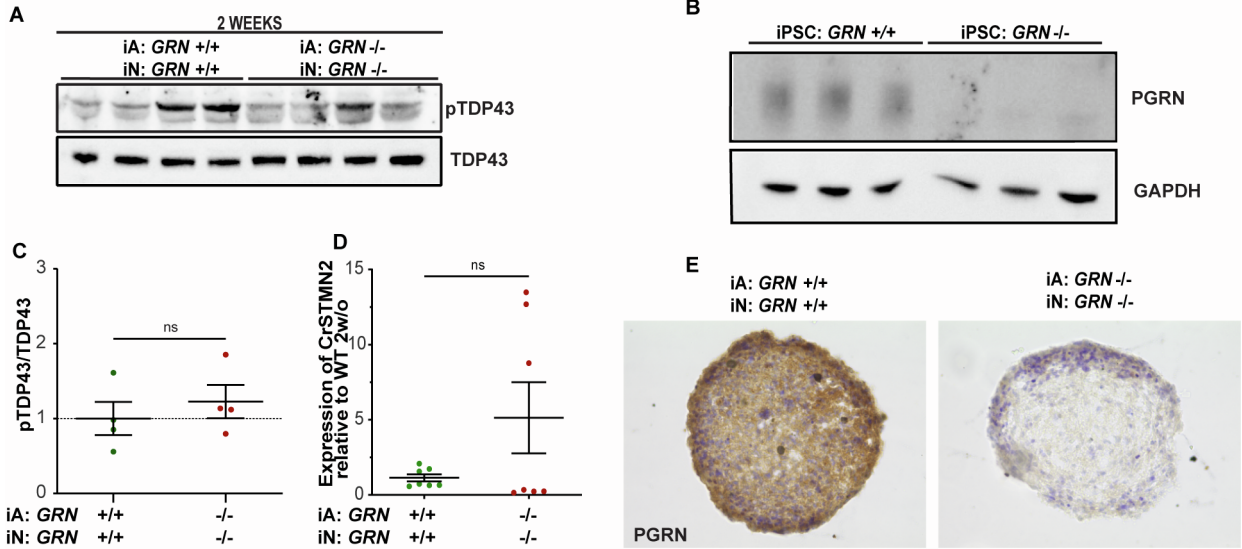
cDNA samples were treated for genomic DNA contamination using TURBO DNA-free kit (Life Tech Cat#AM1907) per manufacturer's instructions. The cDNA was then diluted to a concentration of 5 ng/ μl and 4 μl of each sample (total of 20 ng) were aliquoted in a white walled 96 well plate (Thermo Scientific) in technical duplicates. Samples were processed using PrimeTime std qPCR Assay (IDT) and IDT commercial standard conjugated primers for each of the genes analyzed except for cryptic STMN2 for which primers were designed by Kevin Eggan's lab and kindly shared with us (Forward: CTCAGTGCCTTATTTCAGTCTTCTC, Probe: TCAGCGTCTGCACATCCCTACAAT, Reverse: TCTTCTGCCGAGTCCCAT). The quantitative PCR was run on Bio-Rad C1000 Thermal Cycler/CF96 Real-Time System following manufacturer's instructions. Data analysis was carried out applying the Pfaffl mathematical model for relative transcript quantification (Pfaffl, 2001) using RNA18S as a housekeeping gene.

RNA sequencing and analysis

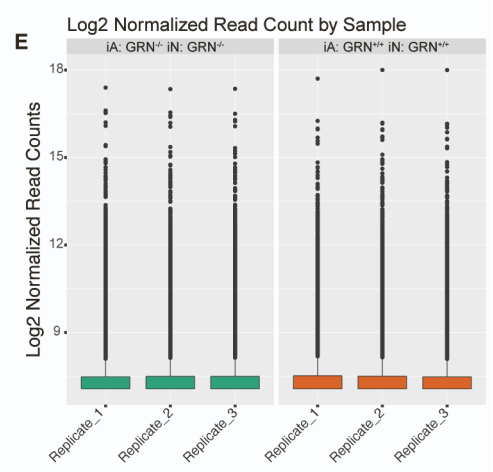
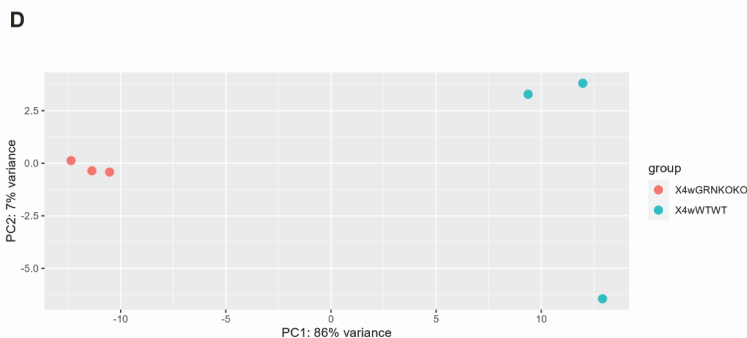
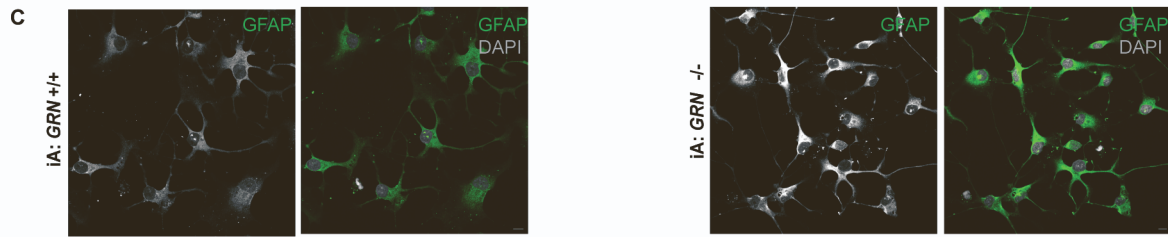
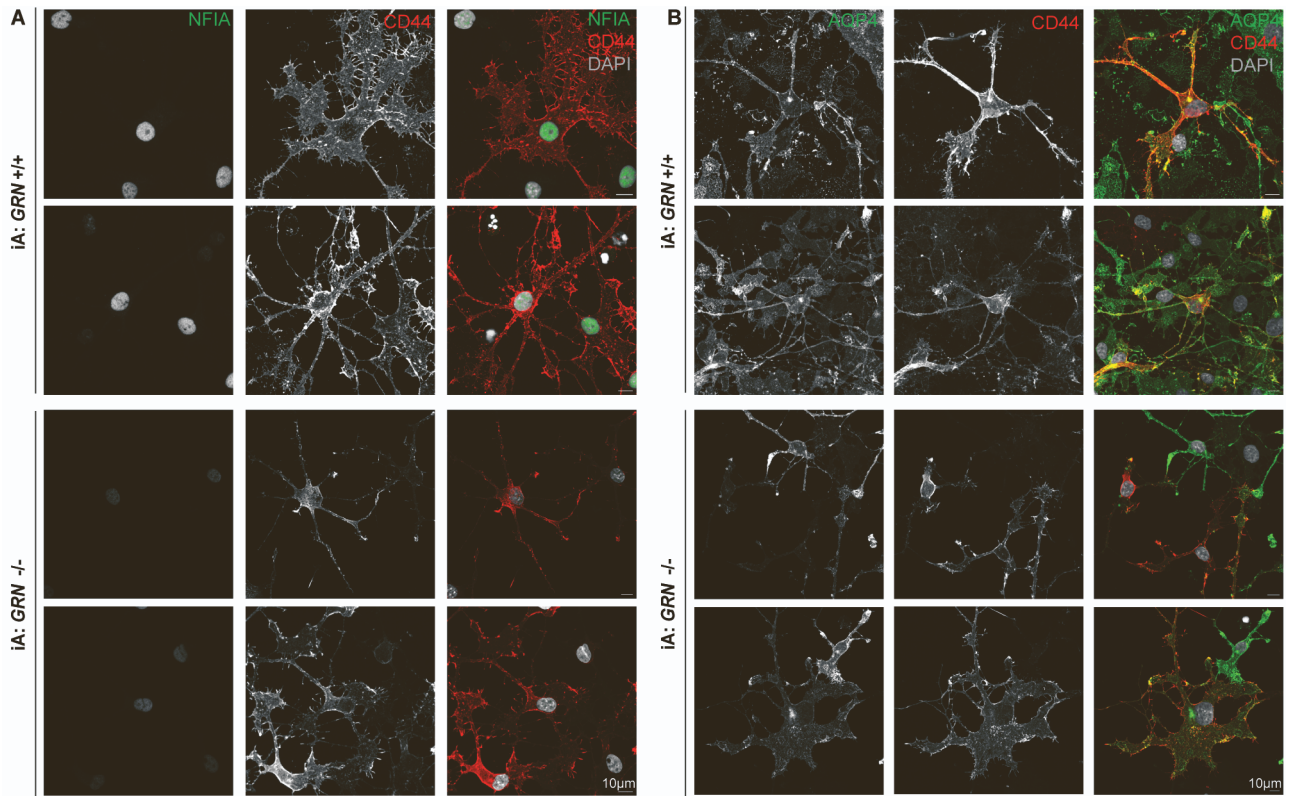
RNA integrity was analyzed on an Agilent 2100 Bioanalyzer using RNA 6000 Nano kit (Agilent, 5067-1511). Only samples with an RNA integrity number (RIN) ≥ 9.4 were used to perform bulk RNA sequencing. Nugen Universal Plus (Tecan) was used as a library kit and libraries were sequenced on a SP300 flow cell of the Illumina NovaSeq 6000 machine with a paired-end 150 bp sequencing strategy (average depth 90 million reads/sample) at UCSF Genomics Core Facility. Genome was aligned to Ensembl Human.GRCh38.103. Kallisto 0.46.01 was used to generate transcript abundance files for each sample. Transcript counts files for each sample were generated using txImport and transcript differential analysis was performed using DESeq2 v1.24.0. A total of 6 samples were spread across two conditions.

Phagocytosis assay

Astrospheres were dissociated and counted. 10 wells at ~50k cells/well were plated in a 96 well/plate (~500k samples per condition). Astrocyte maturation was performed as previously described in iAstrocyte validation. One set of GRN^{-/-} astrocytes was treated with PGRN 1 µg/ml (Adipogen, AG-40A-0188Y) every 72 hours. On the day of analysis, a subset of samples per condition were pre-treated with Cytochalasin D 10µM (Sigma #C2618) for 15 minutes to inhibit actin polymerization. Phagocytosis assay was performed as previously described (Dräger et al., 2022). Briefly, all samples were incubated with pHRodoRed-labeled synaptosomes at a concentration of 1 mg/ml in astrocyte media. Synaptosomes were isolated from fresh Innovative Grade US Origin Rat Sprague Dawley Brain (Innovative Research, Inc.; Cat. No. IGRTSDBR) with the Syn-PER[™] Synaptic Protein Extraction Reagent (Thermo Scientific[™]; Cat. No. 87793) according to the manufacturer's protocol and then labelled with pHrodo[™] Red, succinimidyl ester (pHrodo[™] Red, SE) (ThermoFisher Scientific; Cat. No. P36600) as previously described (Dräger et al., 2022). Cells were washed twice with DPBS, dissociated, resuspended in ice-cold DPBS, and analyzed via flow cytometry. Flow cytometry data were analyzed using FlowJo (<https://www.flowjo.com/>).



Supplementary figure 1. A) Western blot of mbOrg whole lysate showing similar expression on pTDP-43 in *GRN*^{-/-} and *GRN*^{+/+} mbOrg when normalized to total TDP-43 at two-week timepoint. C) Western blot quantification showing no difference in expression on pTDP-43 in *GRN*^{-/-} compared to *GRN*^{+/+} mbOrgs when normalized to total TDP-43 (n=4, unpaired t test, two tailed, p=ns, each n represents ~50 mbOrgs and was repeated independently four times). B) Western blot of WTC11 iPSCs whole lysate confirming GRN knock out in *GRN*^{-/-} WTC11 lines. D) Quantification of CrSTMN2 expression using qPCR showing no difference in CrSTMN2 expression in *GRN*^{-/-} compared to *GRN*^{+/+} mbOrg after two weeks in culture (n=7±, unpaired t test, two tailed, p<0.001, each n represents ~50 mbOrgs and the experiment was repeated independently three times). E) Brightfield images of PGRN immunostaining in 3D cultures at 2-week timepoint showing the loss of PGRN in *GRN*^{-/-} pure combination compared to *GRN*^{+/+} pure combination. F) Representative ICC images of 2D neuronal cultures after for weeks. Cells were stained for TDP-43, MAP2 and pTDP-43 (scale bar 10µm). G) Quantification of CrSTMN2 expression using qPCR showing no difference in CrSTMN2 expression in *GRN*^{-/-} compared to *GRN*^{+/+} 2D neuronal cultures after four weeks in culture (n=5±, unpaired t test, one way ANOVA followed by multiple comparison, ns p>0.05, each n represents ~1x10⁶ cells and was repeated independently three times). H and K) Quantification of MERTK and MEGF10 expression using qPCR showing significantly MERTK and MEGF10 lower expression in *GRN*^{-/-} compared to *GRN*^{+/+} 2D cocultures after four weeks in culture. MERTK and MEGF10 expression is not rescued when *GRN*^{-/-} co-cultures were treated with exogenous PGRN(n=4 or n=9 respectively, one way ANOVA followed by multiple comparison, **p<0.005, ****p>0.00005, each n represents ~1x10⁶ cells and was repeated independently three times). I and J) quantification of extranuclear TDP-43 per mm² (I) and TDP-43 nuclear intensity per mm² (J) in *GRN*^{-/-} compared to *GRN*^{+/+} mbOrg. Each dot represents one independent mbOrg (*GRN*^{+/+} n=4, *GRN*^{-/-} n=6, unpaired t test, two tailed, p<0.05, each n is one mbOrg, and the experiment was repeated independently 3 times). For all graphs data are represented as mean ± SEM.



F

GRN +/+ Parental cccgccagGCTGTGTGCT GCGAGGATCGC CAGCACTGCT GCCCGGCTGG CTACACCTGC AACGTGAAG-----GCTCGATCCTGCGA GAA

Parental cccgccagGCTGTGTGCT GCGAGGATCGC CAGCACTGCT GCCCGGCTGG CTACACCTGC AACGTGAAG-----GCTCGATCCTGCGA GAA

Exon 12

GRN -/- Allele 1 cccgccagGCTGTGTGCT GCGAGGATCGC CAGCACTGCT GCCCGGCTGG CTACACCTGC AACGTGAAG-----GCTC----- GAA

Allele 2 cccgccagGCTGTGTGCT GCGAGGATCGC CAGCACTGCT GCCCGGCTGG CTACACCTGC AACGTGAAGGCTCGATGCTCGATCCTGCTA GAA

10 bp deletion

7 bp insertion

1 bp mutation

Supplementary figure 2. A) Representative ICC images of 2D iA cultures stained for NFIA, CD44 and DAPI (scale bar 10 μ m) after one week differentiation B) Representative ICC images of 2D iA cultures stained for AQP4, CD44 and DAPI (scale bar 10 μ m) after 1 week differentiation. C) Representative ICC images of 2D iA cultures stained for GFAP and DAPI (scale bar 10 μ m) after one week differentiation. D) Principal components plot indicating distance between samples with principal component 1 (PC1) vs principal component 2 (PC2) and highlighting samples separation by genotype. E) Boxplots by sample for normalized read count values for all six analyzed samples. F) Diagram showing the *GRN* region in the WTC11iPSC line that was modified in the *GRN*^{-/-} WTC11 iPSC. The modification results in a 10 base pair deletion (allele 1) and a 7+1 base pair insertion (allele 2) in Exon 12. These nonsense variants lead to the formation of a premature stop codon and a transcript that is degraded by nonsense mediated decay resulting in a *GRN* knock out iPSC line. For all graphs data are represented as mean \pm SEM.

References

Pfaffl, M. W. (2001). A new mathematical model for relative quantification in real-time RT-PCR. *Nucleic Acids Research*, 29(9), e45. <https://doi.org/10.1093/nar/29.9.e45>

Schindelin, J., Arganda-Carreras, I., Frise, E., Kaynig, V., Longair, M., Pietzsch, T., Preibisch, S., Rueden, C., Saalfeld, S., Schmid, B., Tinevez, J.-Y., White, D. J., Hartenstein, V., Eliceiri, K., Tomancak, P., & Cardona, A. (2012). Fiji: an open-source platform for biological-image analysis. *Nature Methods*, 9(7), 676–682. <https://doi.org/10.1038/nmeth.2019>